Theses and Dissertations

Summer 2015

Progressing the understandings of sea spray aerosol through model systems and nem Methods of analysis

Joshua Ryan Grandquist
University of Iowa

Recommended Citation

PROGRESSING THE UNDERSTANDINGS OF SEA SPRAY AEROSOL THROUGH
MODEL SYSTEMS AND NEW METHODS OF ANALYSIS

by

Joshua Ryan Grandquist

A thesis submitted in partial fulfillment
of the requirements for the Master of
Science degree in Chemical and Biochemical Engineering
in the Graduate College of
The University of Iowa

August 2015

Thesis Supervisor: Professor Vicki H. Grassian

Graduate College
The University of Iowa
Iowa City, Iowa

CERTIFICATE OF APPROVAL

_____

MASTER'S THESIS

_____

This is to certify that the Master's thesis of

Joshua Ryan Grandquist

has been approved by the Examining Committee
for the thesis requirement for the Master of Science
degree in Chemical and Biochemical Engineering
at the August 2015 graduation.

Thesis Committee: _____
                     Vicki H. Grassian, Thesis Supervisor

                   _____
                     Charles O. Stanier

                   _____
                     Alexei V. Tivanski

To my parents, Ann, Jim, and Sue, for everything you have done for me, which could fill a whole other thesis.
To all of my friends and family, you all have helped shape me into the man I am today.

Nothing in the world is worth having or worth doing unless it means effort, pain, difficulty… I have never in my life envied a human being who led an easy life. I have envied a great many people who led difficult lives and led them well.

Theodore Roosevelt

ACKNOWLEDGEMENTS

ABSTRACT

Currently, there exists a great deal of uncertainty regarding atmospheric aerosols and the role that they play within the Earth's atmosphere. It is known that atmospheric aerosols can play a role in the Earth's climate by scattering and absorbing solar radiation or acting as a cloud condensation nuclei. The purpose of this work is to obtain an improved understanding of the chemistry of atmospheric aerosols to better determine their impacts the environment, air quality, and climate.

This work revolves around one specific type of atmospheric aerosol, i.e. sea spray aerosol. Sea spray aerosol is generated via breaking waves, through wind-driven mechanisms. Ocean water covers roughly 71% of the Earth's surface, and from this over 1300 Tg of sea spray aerosols is emitted into the atmosphere every year. However, until recently, the study of sea spray was very challenging and often inconclusive due to the inability to filter background particles out. In this work, the understanding of sea spray aerosol is progressed by taking a two-pronged approach. First, this work focuses on the study of model systems of simple ocean surfactants and NaCl and the change in chemistry that occurs when the two are in the presence of each other. Second, sea spray samples generated during a biological bloom are isolated and analyzed. Using this two pronged approach, it is shown that model systems can provide supporting evidence for hypotheses created from trends discovered in more complex samples. Finally, common aerosol generation, storage, and analysis techniques are studied in order to improve our understanding of their effects on aerosol particles.

PUBLIC ABSTRACT

For many decades, global warming has been a worldwide concern due to its potential harmful effects on society. In addition to the more commonly known cause of this global phenomenon, greenhouse gases, another important component of the Earth's atmosphere is atmospheric aerosols. Atmospheric aerosols are small, solid and/or liquid particles suspended in the air that vary greatly in size and chemical composition. Much of these variations are a result of the wide variety of natural and man-made sources that emit aerosols into the atmosphere. Like greenhouse gases, these particles can significantly influence the Earth's climate. However, in contrast to greenhouse gases, it is not well understood as how and to what extent, do aerosols impact the climate.

In this work, we learn more about one of the most abundant types of atmospheric aerosol, namely sea spray. Although invisible to the naked eye, millions of tiny sea spray aerosols are constantly being released from the Earth's ocean into the atmosphere via breaking waves. Here we take a look at how the chemical components and processes of the ocean can alter the properties of sea spray aerosols. This knowledge will bring us one step further in understanding the influence these aerosols have on our climate.

TABLE OF CONTENTS

LIST OF TABLES

Table

Figure

CHAPTER 1 – INTRODUCTION

The atmosphere is not only comprised of gases, but it also contains liquid and solid matter in the form of particles. These particles are commonly referred to as atmospheric aerosols [Boucher et al., 2013]. These particles have a wide range of sizes, shapes, chemical composition, and effects on the atmosphere.

Aerosols are generally broken into two types, anthropogenic and natural, based on their form of origin. Anthropogenic aerosols are derived from manmade sources and are often attributed to transportation or industrial processes, like fossil fuel and biomass burning [Pacyna, 2007]. Natural aerosols originate from naturally occurring processes, e.g. via wind-blown dust, volcanic eruptions, or wave crashing, for example [Viana et al., 2013]. Figure 1.1 shows a variety of pathways and sources of some of the most common atmospheric aerosols and gases.

While it is hard to determine the exact amount of atmospheric aerosols in the atmosphere, it is estimated that natural aerosol sources produce around 3,100 Tg/year, and anthropogenic sources account for 460 Tg/year. Major sources of natural atmospheric aerosols include soil dust, conservatively estimated at 1500 Tg/year reaching the atmosphere, and sea spray, which this work is concentrated on, estimated at 1300 Tg/year. Secondary aerosols, i.e. aerosols produced via gas-to-particle conversion, is the major source of anthropogenic aerosols, producing around 330 Tg/year. This conversion is what happens when certain gas-phase reactions result in the formation of low-vapor-pressure reaction products, which allows them to exist at high super-saturation levels, condense, and form particles. Combustion products are a good example of this pathway [Hinds, 1999]. While it may seem that when the total mass of anthropogenic aerosols is only ~13% of the total atmospheric aerosol emissions each year, this number has steadily increased since the Industrial Revolution in the mid-18th century [Stocker et al., 2013].
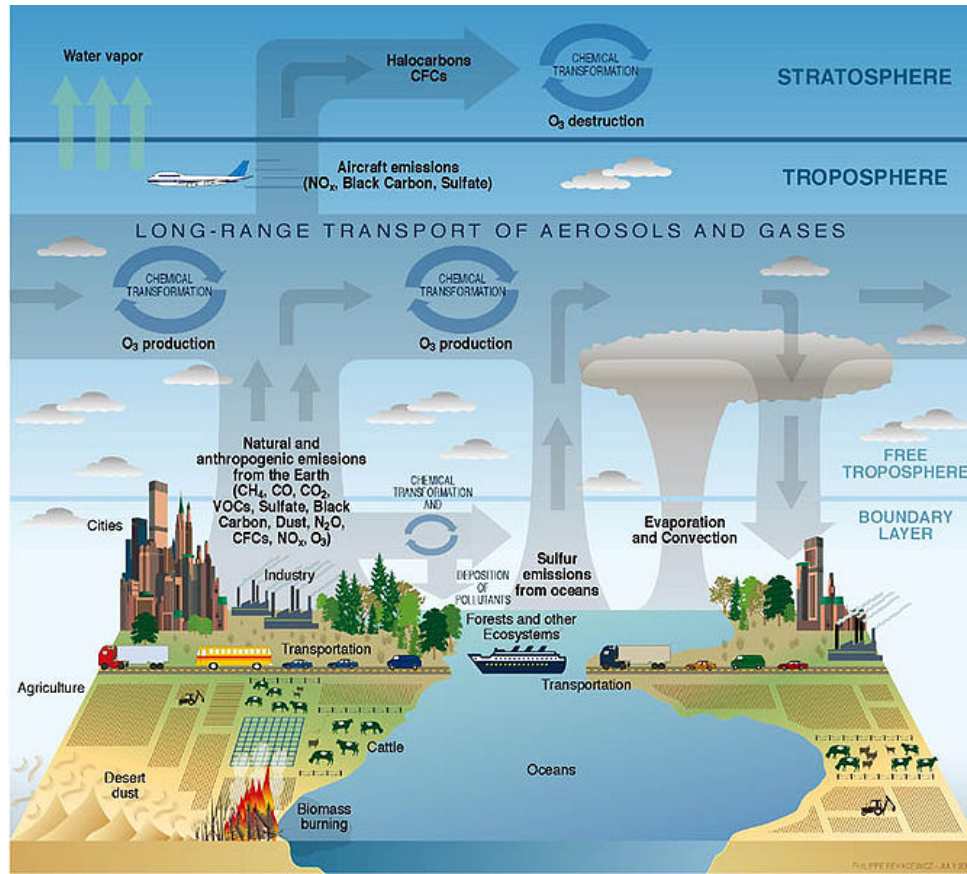
Figure 1.1 Schematic of chemical and transport processes related to atmospheric composition. (Public domain figure taken from Albritton et al., 2003).

Despite the small sizes of these particles, often ranging from a few nanometers to a couple of microns in diameter, they can greatly affect the atmosphere in a multitude of ways. Figure 1.2 demonstrates the direct, indirect, and semi-direct effects of atmospheric aerosols. Direct effects of aerosols are the result of atmospheric particles scattering and absorbing the incoming solar and infrared radiation in the atmosphere. The scattering of the incoming radiation back into space will cause a cooling effect on the surface of the Earth and the atmosphere. The absorption of radiation by some particles, like black carbon, will result in the increased temperature of the atmosphere [Penner et al., 2001]. The amount of light scattered or absorbed by the aerosol is dependent upon the properties of the aerosol [Seinfeld and Pandis, 2006].

2
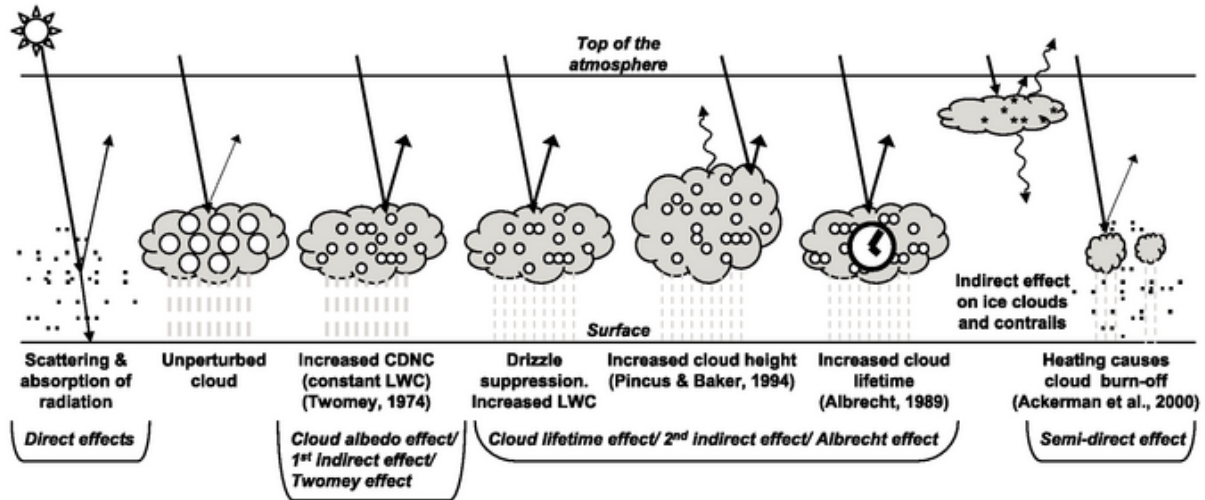
Figure 1.2 Schematic diagram showing the various radiative mechanisms associated with cloud effects that have been identified as significant in relation to aerosols (modified from Haywood and Boucher, 2000). The small black dots represent aerosol particles; the larger open circles cloud droplets. Straight lines represent the incident and reflected solar radiation, and wavy lines represent terrestrial radiation. The filled white circles indicate cloud droplet number concentration (CDNC). The unperturbed cloud contains larger cloud drops as only natural aerosols are available as cloud condensation nuclei, while the perturbed cloud contains a greater number of smaller cloud drops as both natural and anthropogenic aerosols are available as cloud condensation nuclei (CCN). The vertical grey dashes represent rainfall, and LWC refers to the liquid water content. (Public domain figure taken from Forster et al., 2007).

Atmospheric particles can also have indirect effects on the atmosphere. Atmospheric aerosols can act as cloud condensation nuclei (CCN), or "cloud seeds". These seeds allow for favorable conditions in the atmosphere for water to condense on and form clouds. A greater aerosol concentration leads to a greater number of cloud condensation nuclei, which in turn, leads to more water droplets in the cloud, and therefore an increase in cloud albedo [Seinfeld and Pandis, 2006]. Cloud albedo is how bright a cloud appears; the brighter the cloud, the more solar radiation it is reflecting, and is therefore creating a greater cooling effect in the atmosphere. These types of clouds are often found downwind of heavily polluted areas [Rosenfeld and Woodley, 2001]. Additionally, aerosols can affect the lifetime of clouds. When clouds have more CCN, this leads to a cloud having increased concentrations of smaller droplets. In order for clouds to precipitate rain, a relatively large threshold of condensed water must be met on the CCN. When there are more seeds to condense onto, this process takes longer, thus delaying the onset of precipitation.

3
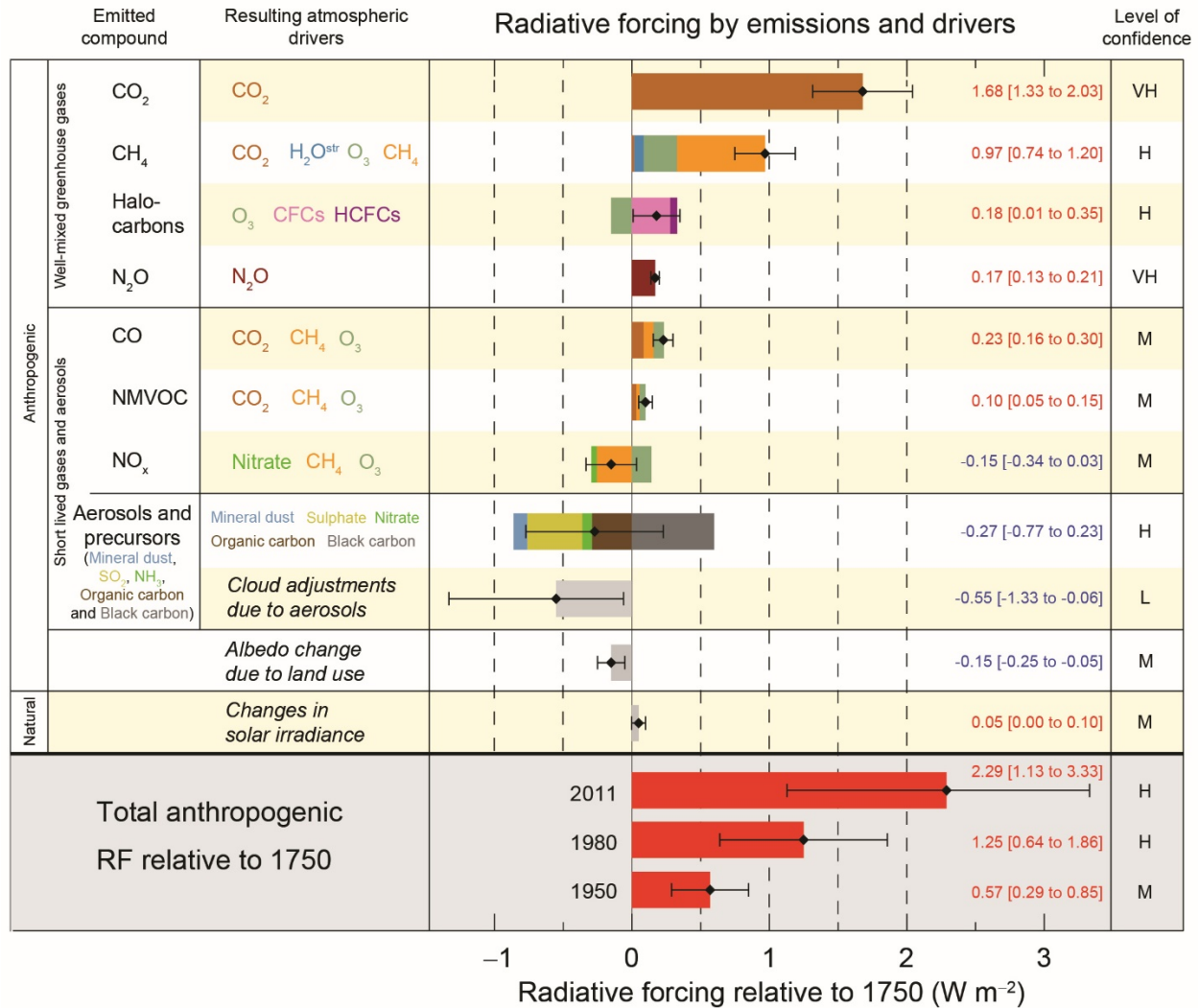
Figure 1.3 Radiative forcing estimates in 2011 relative to 1750 and aggregated uncertainties for the main drivers of climate change. Values are global average radiative forcing (RF14), partitioned according to the emitted compounds or processes that result in a combination of drivers. The best estimates of the net radiative forcing are shown as black diamonds with corresponding uncertainty intervals; the numerical values are provided on the right of the figure, together with the confidence level in the net forcing (VH – very high, H – high, M – medium, L – low, VL – very low). Albedo forcing due to black carbon on snow and ice is included in the black carbon aerosol bar. Small forcing due to contrails (0.05 W m–2, including contrail induced cirrus), and HFCs, PFCs and SF6 (total 0.03 W m–2) are not shown. Concentration-based RFs for gases can be obtained by summing the like-colored bars. Volcanic forcing is not included as its episodic nature makes is difficult to compare to other forcing mechanisms. Total anthropogenic radiative forcing is provided for three different years relative to 1750. (Public domain figure taken from IPCC, 2013).

Therefore, the longer the cloud lifetime, the more it will affect the radiative balance of the atmosphere [Denman et al. 2007].

Lastly, the semi-direct effect is referred to as the result on the formation and lifetime of clouds due to the effects of when aerosols absorbs solar radiation. The absorption modifies the air

4

temperature, humidity, and vertical stability of the air column, which results in altered formation and lifetime of clouds [Goosse et al., 2008].

Figure 1.3 summarizes the components of radiative forcing that can take place within the Earth's atmosphere. The biggest effect on the radiative balance is greenhouse gases, specifically CO_2, with almost a +1.7 W/m^2 increase of radiative forcing due to CO_2 since 1750. Much is known about the effects of greenhouse gases on the atmosphere, as demonstrated by the small error bars on the bar graph. The next largest influence is aerosols. Unlike greenhouses gases, less is known and understood about atmospheric aerosols and their impacts on Earth's climate, as shown by the wide error bar margins on Figure 1.3 and the fact that there is not a very high certainty in the level of understanding [IPCC, 2013].

The focus of this thesis is on sea spray aerosols. Sea spray aerosols are generated through wave breaking of sea water, causing bubble bursting, and play a significant role in the tropospheric chemistry and atmospheric environment [Laskin et al., 2012]. The ocean covers approximately 71% of the Earth's surface and therefore provides a constant, significant, and yet still relatively unknown source of atmospheric aerosols [Wex et al., 2010]. What was once previously believed to be comprised of mostly NaCl salt with little to no other chemical components, has been shown be much more chemically complex [Prather et al., 2013]. The NSF Center for Aerosol Impacts on Climate and the Environment (CAICE) focuses on answering the questions involving how multifaceted aerosols, specifically sea spray aerosols, impact the environment, air quality, and climate. Led by Dr. Kimberly A. Prather, Dr. Vicki H. Grassian, and Dr. Timothy H. Bertram, CAICE brings together researchers from nine universities all over the United States, all specialized in different aspects of aerosol research. Centered on the campus of the University of California, San Diego, this conglomeration of over 40 graduate students and post docs, uses computational

tools and state of the art instrumentation to focus on reducing the large gap of knowledge in the crucial area of aerosol chemistry. Researchers are using new innovative tools, such as the linear wave channel (discussed in Chapter 3 and 4) at the Scripps Institute of Oceanography in La Jolla, CA and the Marine Aerosol Reference Tank (discussed in Chapter 4), to generate sea spray aerosols using the same natural mechanisms as those occurring in the ocean. The pristine particles are analyzed and experimented on using many different on- and off-line analysis techniques, from Raman spectroscopy and electron microscopy to mass spectrometry. These findings help steer the direction of CAICE and the subsequent experiments that probe the chemical complexity of these aerosols. Though only been an active center for less than five years, CAICE has already made many significant impacts and innovations in the area of aerosol chemistry [Prather et al., 2013; Ault et al., 2013; Stokes et al., 2013; Ault et al., 2013; Collins et al., 2013; Ebben et al., 2013; Guasco et al., 2014; Collins et al., 2014; Laskina et al., 2015; Wang et al., 2015].

As a part of CAICE, this thesis focuses on several different aspects of sea spray aerosol. Chapter 2 will focus on model system studies of common ocean surfactants and the interactions with NaCl aerosols. This chapter lays the ground work for Chapter 3, where the trends of collected seas spray aerosol field sample, discovered by microscopy techniques, are compared to those seen in model systems. Lastly, Chapter 4 will discuss the new method developments made in aerosol generation, storage conditions, and sample analysis.

CHAPTER 2 – MODEL SYSTEMS

In order to fully understand and explain the varying levels of chemical complexity that are seen in environmental aerosols, laboratory experiments under controlled conditions are needed. These experiments can provide the scientific basis for understanding fundamental processes that occur in the environment, such as the property changes of aerosols generated in polluted vs clean areas. Laboratory experiments allow for control of all aspects and variables, thus providing a way to confirm or disprove the initial hypothesis on processes occurring in the environment.

2.1 Chloride Depletion of NaCl by Model Systems

Sea spray aerosol particles undergo heterogeneous reactions in the atmosphere [Finlayson-Pitts, 2003]. With these reactions, atmospheric aerosols can undergo changes in their physicochemical properties. Reacted particles may change their water uptake properties, optical properties, and ability to act as a cloud condensation nuclei (CCN) [Laskin et al., 2012]. One reaction that has been recently discussed is the acid displacement reaction of NaCl with atmospheric acidic gases, expressed in the generalized form:

$$NaCl_{(aq)} + HA_{(aq,g)} \rightarrow NaA_{(aq)} + HCl_{(g)} \tag{R 2.1}$$
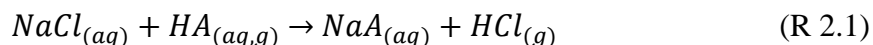
where NaCl is an aqueous solution containing any chloride salts of seawaters, and HA represents any relevant atmospheric acids, such as nitric and sulfuric acids. This depletion in chloride has been shown in many different field studies, ranging from areas where there is a range of pollution levels and remote areas, where the particles are expected to be pristine [Laskin et al., 2002, 2005; Newberg et al., 2005]. In literature, some attribute part of this chloride deficiency to the formation of inorganic salts (e.g. sulfates and nitrates) [Keene et al., 1990; Kerminen et al., 1998], and the heterogeneous and interface chemistry of sea spray aerosols with trace atmospheric gases [Finlayson-Pitts, 2003]. Recently, Laskin et al. [2012] have suggest that anthropogenic secondary
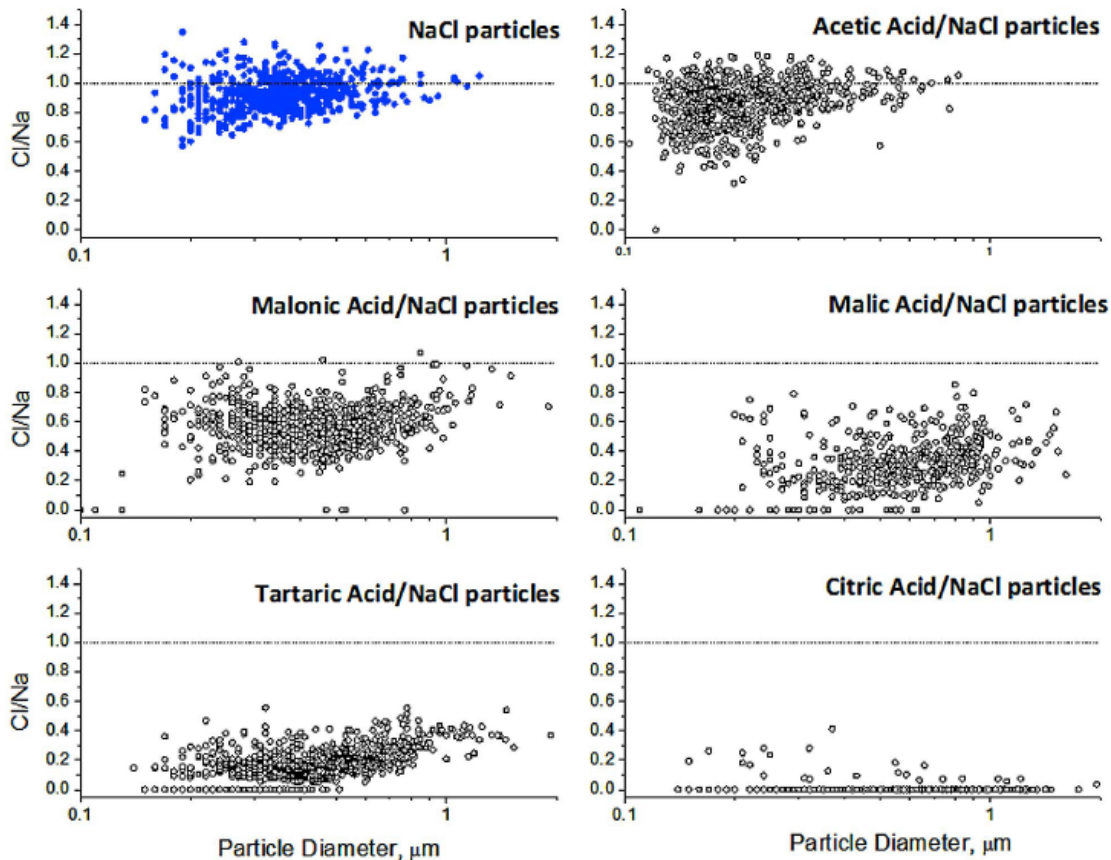
Figure 2.1 Values of Cl/Na ratios measured by CC-SEM/EDX in dry residues of NaCl, and mixed organic acid/NaCl (1/1 molar ratio) particles. Values of Cl/Na below unity (dashed lines) indicate Cl depletion by organic acids. (Figure taken with permission from Laskin et al. 2012).

organic aerosols (SOA) are abundant and may facilitate acid displacement reactions that liberate HCl (g). It was further suggested that the chemical composition, hygroscopic, and optical properties of these particles may change in ways that have yet to be explored. Laskin et al. went on to show that particles generated from a nebulized 0.5 M solution of 1/1 molar ratio of NaCl and a variety of short chain organic acids, can be depleted in chloride. Laskin used common atmospheric mono-, di-, and tricarboxylic acids, including acetic, malonic, malic, tartaric, and citric acid. Figure 2.1, taken from Laskin et al. [2012], shows the EDX results of the Cl/Na ratio of hundreds of individual reacted particles for all of the acids studied. For the unreacted NaCl sample, the Cl/Na ratio is measured to be one, as based on the stoichiometry. The other scatter

الٱمٱرٱة للاستشارات

www.manaraa.com

NaCl:Acid Molar Ratio	Acid	pH
3:1	Malic	1.97
1:1	Malic	1.96
1:3	Malic	1.69
3:1	Hexanoic	3.04
1:1	Hexanoic	3.14
1:3	Hexanoic	3.12
3:1	Nonanoic	3.86
1:1	Nonanoic	3.85
1:3	Nonanoic	3.97
3:1	Palmitic	4.74
1:1	Palmitic	4.62
1:3	Palmitic	4.18

Table 2.1 The measured pH of each solution used to generate the sample aerosol particles.

plots show that these organic acids cause a decrease in Cl/Na ratio. As a result, we offer a slightly

modified version of the reaction:

$$NaCl_{(aq)} + R - COOH_{(aq)} \rightarrow R - COO^-Na^+{}_{(aq)} + HCl_{(g)} \qquad \text{(R 2.2)}$$
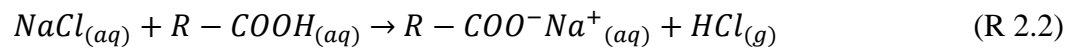
For this thesis, we conduct experiments similar to Laskin et al. [2012] and expand the number and

types of organics acids investigated. Below are the results of analysis of individual particles

produced from 3/1, 1/1, and 1/3 molar ratio solution of NaCl and common oceanic surfactant acids:

malic, hexanoic, nonanoic, and palmitic acids. With the results reported in this chapter, we propose

another mechanism by which particles become depleted in chlorine, R 2.2. This reaction formula

is similar to that proposed by Laskin et al., where NaCl is an aqueous solution containing any

chloride salts of seawaters, but HA has been replaced with R-COOH, which represents any

relevant aqueous ocean surfactant. The change in formula is slight, but we propose that chlorine

depleted particles may be due not only to the heterogeneous reaction of sea spray aerosol particles

in the atmosphere, but also can occur because of the reaction between acidic ocean surfactants and
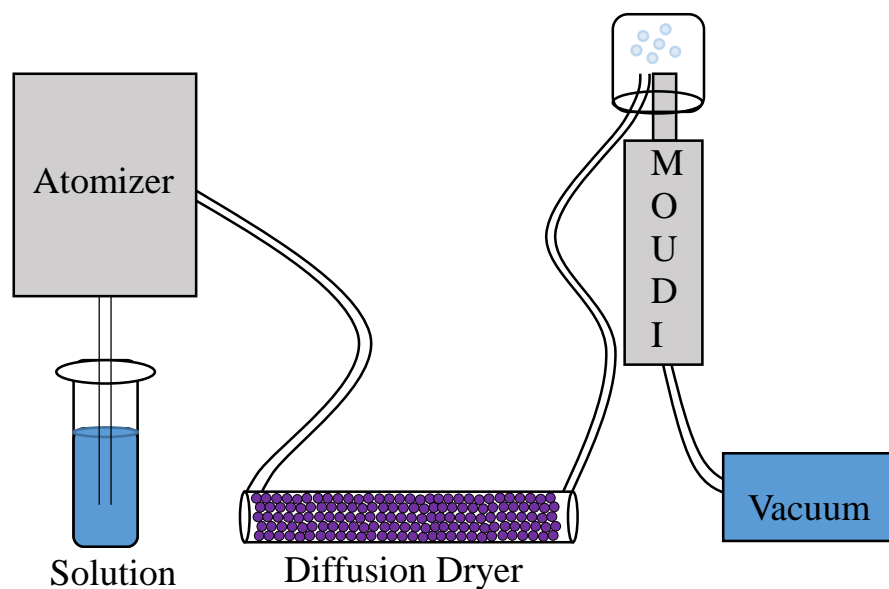
Figure 2.2 A schematic of the aerosol generation setup for the collection of model system particles.

sea salts upon the formation of sea spray aerosol. In this chapter, we provide experiments on carboxylic acids in ocean sea water.

2.1.1 Experimental Setup

2.1.1.1 Aerosol Sample Preparation

Particles were generated from aqueous solutions of NaCl and organic acids mixed at three different molar ratios: 3/1, 1/1, and 1/3. NaCl (Fisher Scientific, 99.8%), malic acid (Alfa Aesar, 98.0%), hexanoic acid (Sigma-Aldrich, ≥99.5%), nonanoic acid (Sigma-Aldrich, ≥97.0%), and hexadecanoic (palmitic) acid (Sigma-Aldrich, ≥99.0%) were all used without further purification. All solutions were prepared with deionized water. The pH of each solution can be found in Table 2.1. The particles were generated using a constant output atomizer (TSI, Inc., model 3076). The generated particles were dried down to ~30% RH in a diffusion dryer (TSI, Inc., model 3062) prior to sizing and substrate deposition using a micro-orifice uniform deposit impactor (MOUDI) (MSP, Inc., model 110). Particles were deposited onto copper TEM grids (Ted Pella, Inc.) mounted on the impaction plate of the sixth stage. The range of particles is limited to 300-800 nm due to the analysis of stage 6 of the MOUDI, which collects particles with an aerodynamic diameter size

10

	Radius/ Side 1	Side 2	Radius of Rounded Corner	Area	Perimeter	Circularity Factor
Circle	1			3.14	6.28	1.000
Pentagon	1			1.72	5.00	0.865
Square	1	1		1.00	4.00	0.785
Rounded Square	1	1	0.1	0.99	3.83	0.850
Ellipse	1	1.5		4.71	7.93	0.941
	1	2		6.28	9.69	0.841
	1	3		9.42	13.36	0.663
	1	4		12.57	17.16	0.537
Rectangle	1	1.5		1.50	5.00	0.754
	1	2		2.00	6.00	0.698
	1	3		3.00	8.00	0.589
	1	4		4.00	10.00	0.503
Rounded Rectangle	1	1.5	0.1	1.49	4.83	0.804
	1	2	0.1	1.99	5.83	0.737
Diamond	1	1		1.00	4.00	0.785
Equilateral Triangle	1			0.43	3.00	0.605
Right Triangle	1	1		0.5	3.41	0.539
Line	1			0	1.00	0.000

Table 2.2 The circularity factors of many common sizes and shapes.

range of 0.56-1.0 μm. The reduction in size is due to dehydration upon entering the vacuum chamber. All samples were prepared at room temperature and used within a couple of days after the preparation. Figure 2.2 depicts the experimental setup.

2.1.1.2 Transmission Electron Microscopy with Energy Dispersive X-Ray Spectroscopy

Transmission Electron microscopy (TEM) images were collected using a JEOL JEM-2100F high resolution transmission electron microscope. The field emission TEM installed with Schottky field emission gun, set at an accelerating voltage of 200 kV. The images were acquired using Gatan Orius CCS camera. The TEM is also coupled with an energy dispersive x-ray spectroscopy (EDX) system (Thermo Fischer Scientific), using a Nanotrace Si(Li) X-ray detector. Gatan High Angle Annular Dark Field (HAADF) detector was used for dark field images.

Elemental maps were performed using NORAN System 7 X-ray Microanalysis program. Spectra were acquired for 20 s for each particle analyzed. Chemical analysis results were imported into Microsoft Excel for further investigation. The elements considered in the X-ray analysis were C, N, O, Na, Mg, P, S, Cl, K, and Ca.

2.1.1.3 Image Analysis

Images taken using the TEM where analyzed with ImageJ program. Particles were traced individually and the ImageJ program calculated the diameter, area and perimeter of the particles. This data was imported into Microsoft Excel for further analysis. The area was used to calculate projected-area diameter (d_{PA}) using Eq. (2.1):

$$d_{PA} = \left(\frac{4A}{\pi}\right)^{1/2} \tag{2.1}$$

where A is the area of the particle detected by the ImageJ software. Area and perimeter were also used to determine the circularity factor of particles, using Eq. (2.2):

$$CF = \frac{4\pi A}{P^2} \tag{2.2}$$

where A is the area of the particle and P is its perimeter. The circularity factor is used to determine how close the shape of a particle is to a circle. A particle in the shape of a perfect circle will have a CF = 1.0 and all other shapes will have a CF < 1.0. Table 2.2 provides the circularity factor for many common shapes, for reference.

2.1.2 Results and Discussion

All of the acids used in this work are listed in Table 2.3, along with many of the relevant chemical and physical properties, listed from most soluble to least soluble.

2.1.2.1 Malic Acid

Malic acid is a short chained, dicarboxylic acid that is highly soluble in water, which can be found in Table 2.3. Malic acid is made by all living organisms and often stored in vacuoles of

12
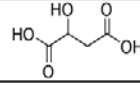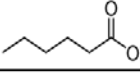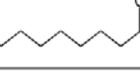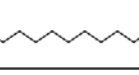
Name of Acid	Chemical Formula	Mono or Dicarboxylic	Structure	Molar Mass	Density (g/mL)	Solubility in Water (g/ L water)	pK$_a$	K$_{a1}$	K$_{a2}$
Malic	HOOCCH$_2$CH(OH)COOH	Di		134.10	1.61	1440	pK$_{a1}$ = 3.40 pK$_{a2}$ = 5.11	3.98E-04	7.76E-06
Hexanoic	C$_5$H$_{11}$COOH	Mono		116.16	0.93	10.2	4.85	1.41E-05	
Nonanoic	CH$_3$(CH$_2$)$_7$COOH	Mono		158.23	0.91	0.284	4.96	1.10E-05	
Palmitic (Hexadecanoic)	CH$_3$(CH$_2$)$_{14}$COOH	Mono		256.40	0.85	8.20E-04	4.78	1.66E-05	

Table 2.3 Physical and chemical properties of all acids used in Chapter 2.

plants, especially tropical plants, which releases it into the surroundings at night as a part of the crassulacean acid metabolism. Additionally, malic acid can also be found within some algae, like *Desmarestia*, a large marine brown algae [Meeuse 1956, 1962]. For these reasons, it is of little surprise that malic acid is a can be commonly found in the ocean, specifically in the sea surface microlayer, where organic compounds are often located in high concentrations [van Pinxteren et al., 2012]. Previous works have also shown malic acid is detected in collected field samples of marine aerosols over the Antarctic [Kawamura et al., 1996], tropics of the Pacific Ocean [Kawamura et al., 1999] and the North Pacific Ocean [Kawamura et al., 1993]. Figure 2.3 A plots the depletion of chloride in individual particles versus the diameter of the aerosol. The y-axis is the average ratio of Cl to Na atomic weight percentages (calculated using the NORAN System 7 program) of individual, reacted particles of a particular diameter ratioed to the average Cl to Na atomic weight percentage ratio, in a 0.1 µm width size bin, of unreacted NaCl. The size bins start at 0.3 µm. For example, a reacted particle with a diameter of 0.361 µm will be ratioed to the average Cl/Na of particles in the 0.3-0.399 µm size bin of pure NaCl, whereas a reacted particle with a diameter of 0.412 µm will be ratioed against the average of the 0.4-0.499 µm size bin of pure NaCl particles. The x-axis is the diameter of the particles in µm. Figure 2.3 B plots the size bin average depletion of chloride in particles versus the bin diameter of the aerosol. The y-axis is the

13
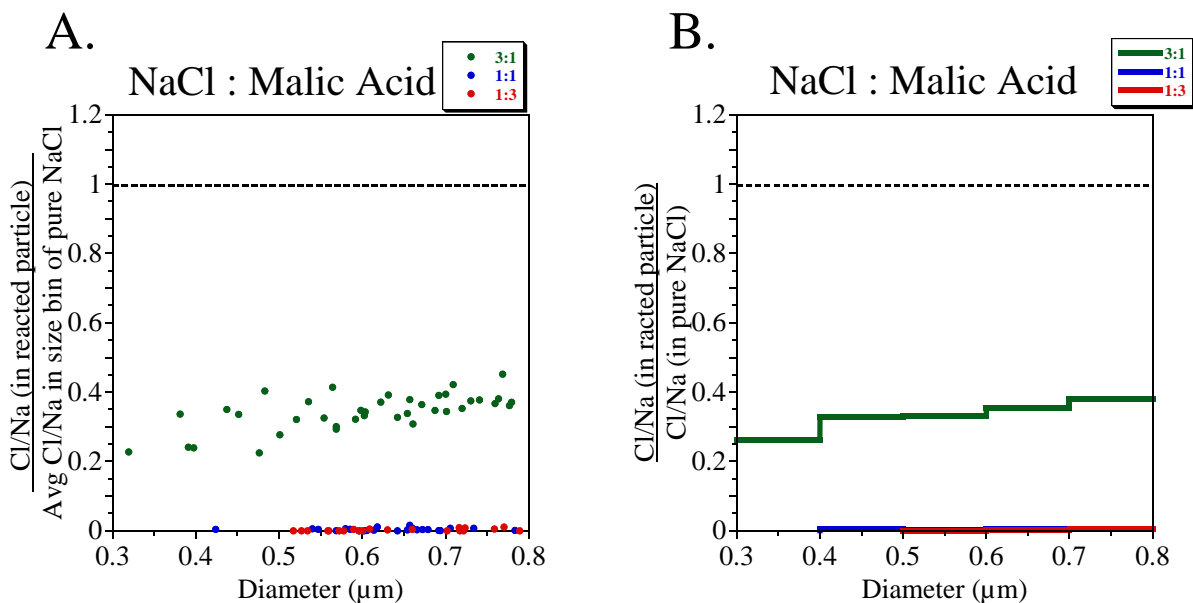
Figure 2.3 TEM/EDX analysis of mixtures of three different NaCl to malic acid molar ratios. Plot A shows the Cl/Na atomic % of individual reacted particle of a particular diameter, ratioed to the average Cl/Na atomic % of pure NaCl particles in the same size bin of the particle. Plot B shows the average Cl/Na atomic % of reacted particle in a particular size bin, ratioed to the average Cl/Na atomic % of pure NaCl particles in the same size bin. The size bins were 0.1 µm in width, starting at 0.3 µm. The dotted line represents the same Cl/Na ratios between the reacted and unreacted NaCl particles.

bin average ratio of Cl to Na atomic weight percentages of the reacted particles ratioed to the Cl to Na ratio of the atomic weight percentages of unreacted NaCl. This number is calculated by taking the mean of the Cl/Na ratios of all of the reacted particles in, for example, the 0.3-0.399 µm size bin, and dividing by the mean of the Cl/Na ratios of all the unreacted particles in the corresponding size bin. The x-axis is the diameter of the particles, separated into bins with 100 nm widths, starting at 0.3 µm. The dotted line represents the same Cl/Na ratios between the reacted and unreacted NaCl particles, in both A and B. Figure 2.3 shows the results of three different molar ratio solutions of NaCl to malic acid. Looking at the plots that show the NaCl-malic acid solution results, there is a significant decrease in the Cl/Na ratio of the resultant particles. When placed into the vacuum chamber of the TEM, the particles shrink due to water loss, resulting in the particles being in the 300-800 nm range due to dehydration (see Chapter 4). The three part salt and one part acid solution shows a substantial decrease in Cl/Na ratio for all particles sizes. Starting around

14
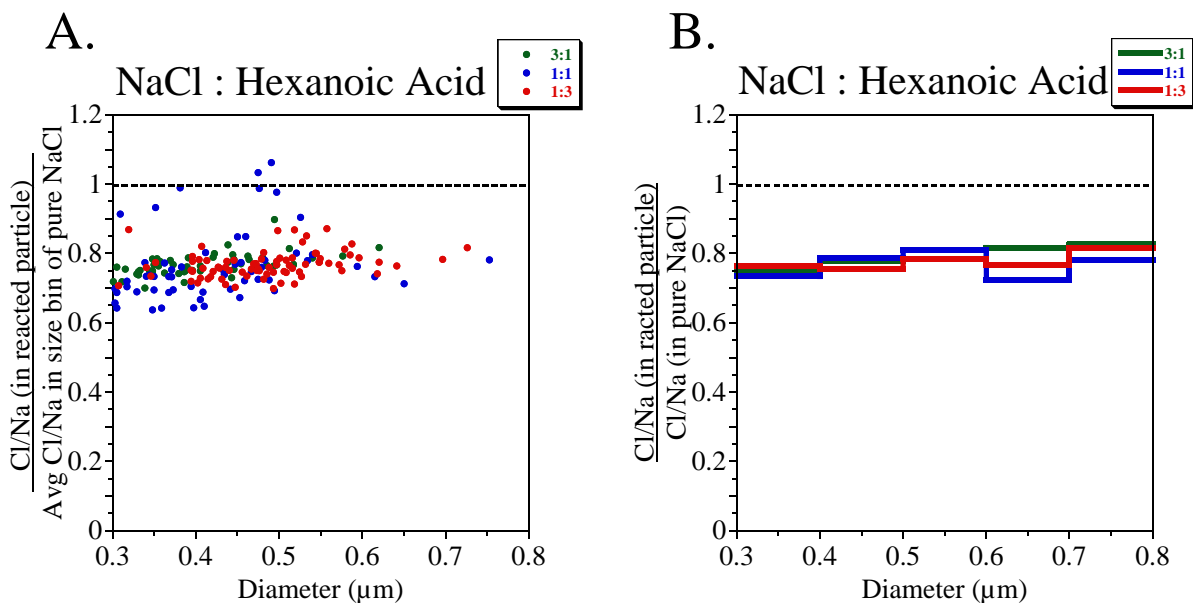
Figure 2.4 TEM/EDX analysis of mixtures of three different NaCl to hexanoic acid molar ratios. Plot A shows the Cl/Na atomic % of individual reacted particle of a particular diameter, ratioed to the average Cl/Na atomic % of pure NaCl particles in the same size bin of the particle. Plot B shows the average Cl/Na atomic % of reacted particle in a particular size bin, ratioed to the average Cl/Na atomic % of pure NaCl particles in the same size bin. The size bins were 0.1 µm in width, starting at 0.3 µm. The dotted line represents the same Cl/Na ratios between the reacted and unreacted NaCl particles.

25% for particles in the 300-400 nm range, the average Cl/Na ratio gradually increases to about 40% with the increasing size ranges. This diameter trend is not surprising, as de Leeuw et al. [2011] point out, smaller particles tend to contain more organic components when compared to larger particles. We attribute the depletion of chloride to the acid displacement formula analogous to R 2.2, where R-COOH represents malic acid. The other two solutions of NaCl to malic acid, one to one and one to three, respectively, show a complete depletion of chloride. When compared to the other acids below, it is evident that malic acid reacts with NaCl very differently than the rest. This could be due to differences in solubility, pK_a, number of carboxylic acids, or the number of available hydroxyl groups available for H^+ donation to the acid displacement reaction mechanism. This suggests that this reaction mechanism can be a significant producer of HCl (g) where malic acid levels are high.

15
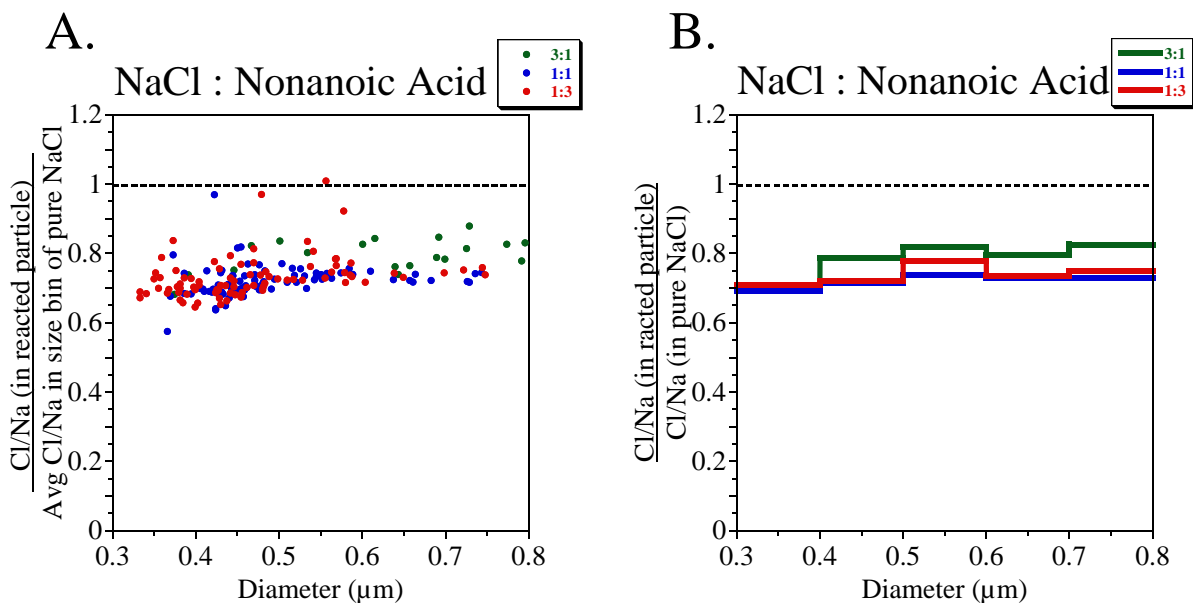
Figure 2.5 TEM/EDX analysis of mixtures of three different NaCl to nonanoic acid molar ratios. Plot A shows the Cl/Na atomic % of individual reacted particle of a particular diameter, ratioed to the average Cl/Na atomic % of pure NaCl particles in the same size bin of the particle. Plot B shows the average Cl/Na atomic % of reacted particle in a particular size bin, ratioed to the average Cl/Na atomic % of pure NaCl particles in the same size bin. The size bins were 0.1 µm in width, starting at 0.3 µm. The dotted line represents the same Cl/Na ratios between the reacted and unreacted NaCl particles.

2.1.2.2 Hexanoic Acid

Hexanoic acid is a six carbon chained monocarboxylic acid. Its solubility in water is one to two orders of magnitude lower than malic acid (sources give a wide range of solubility of malic acid; see Table 2.3), due in part to the longer, nonpolar carbon backbone and singular, polar carboxylic group. Hexanoic acid has a solubility in water of 10.2 g/L. Even though the solubility is low, the organic acid can be often on the ocean surface waters, often from condensation from the atmosphere in coastal areas [Miñambres et al., 2014]. Hexanoic acid has also been shown to reach the aerosol phase in marine particles [Lawler et al., 2014]. Figure 2.4 is plotted similarly to Figure 2.3, but for NaCl-hexanoic acid particles. As shown, there is some significant chloride depletion in the plot, but not nearly as much as that shown for malic acid. This is attributed to a couple reasons. First, based on the pK$_a$ values provided in Table 2.3, the acids will generally be completely dissociated because the sea surface microlayer has an average pH around 8.1 [Zhang

16
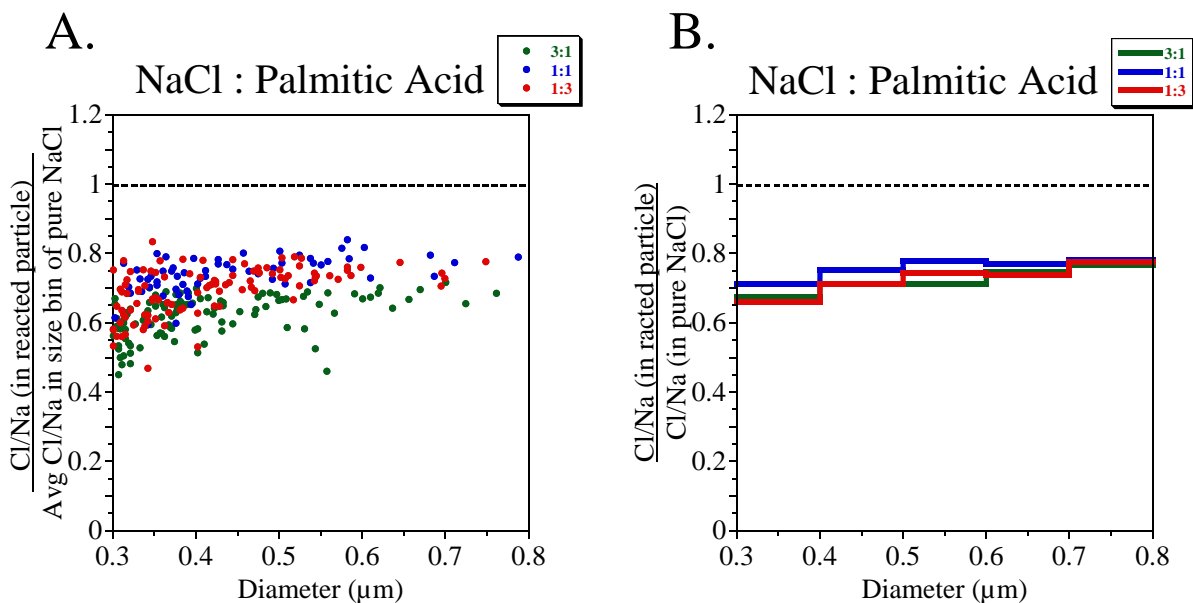
Figure 2.6 TEM/EDX analysis of mixtures of three different NaCl to palmitic acid molar ratios. Plot A shows the Cl/Na atomic % of individual reacted particle of a particular diameter, ratioed to the average Cl/Na atomic % of pure NaCl particles in the same size bin of the particle. Plot B shows the average Cl/Na atomic % of reacted particle in a particular size bin, ratioed to the average Cl/Na atomic % of pure NaCl particles in the same size bin. The size bins were 0.1 µm in width, starting at 0.3 µm. The dotted line represents the same Cl/Na ratios between the reacted and unreacted NaCl particles.

2003]. Hexanoic acid is a monocarboxylic acid and malic acid is a dicarboxylic acid. Secondly, the order of magnitude(s) of lower solubility of hexanoic acid compared to malic acid generally means there will be less overall concentrations of the compound, limiting the interaction between aqueous NaCl and the acid. Given these differences, there is still some depletion of chloride, around 20%. There is little difference between the three solutions of differing molar ratios, suggesting that the reaction will go to completion with even the smallest amount of hexanoic acid present.

2.1.2.3 Nonanoic Acid

Nonanoic acid is a long, nine-carbon fatty acid commonly used in pesticides, but also occurs naturally in plants and animals [Kegley et al., 2010]. While only slightly soluble in water, two orders of magnitude less than that of hexanoic acid, nonanoic acid can still accumulate in the sea surface microlayer. The results of this organic acid mixed with NaCl are shown in Figure 2.5.

17

The plots show similar depletion of chloride to that of hexanoic, ranging from 20-25% for the majority of the particles. The similarities between the two acids can be attributed to the very similar pK_a values of 4.85 and 4.96 for hexanoic and nonanoic, respectively. The similarities suggest that many sea spray aerosol particles will become chloride depleted in the presence of even weakly soluble acids.

2.1.2.4 Palmitic Acid

Lastly, palmitic acid, a long chain 16-carbon length fatty acid, with a single carboxylic acid group on the tail end was investigated. Palmitic acid has a very low solubility in water, 8.20×10^{-4} g/L. Again, this acid is produced within many plants and animals, particularly palm trees (often found in tropical places near water) and certain types of algae [Goecke et al., 2010]. Therefore it is a common ocean surfactant and has recently been specifically linked to marine aerosol particles [Adams et al., 2013], validating the use of it in these experiments. Figure 2.6 shows that palmitic acid and NaCl solutions do produce chloride depleted particles around 20-25%, with very little significant differences between the differing molar ratios. Again, nearly identical depletion percentages is probably due to the similarities in pK_a values between the three acids, because the solubilities are multiple orders of magnitudes different. This result helps support the hypothesis stated in the previous section, in that aerosol particles will become chloride depleted in the presence of acids, regardless of the concentrations.

2.2 Morphological Analysis of Particles

In order to evaluate morphology changes of reacted particles, a quantitative measurement of two-dimensional shape, the circularity factor is used. As described in Section 2.1.1.2, the equation for circularity factor is shown in Eq. (2.2). It is a ratio of the area to the square of the perimeter. This factor provides the opportunity to produce quantitative measurements of morphology. The
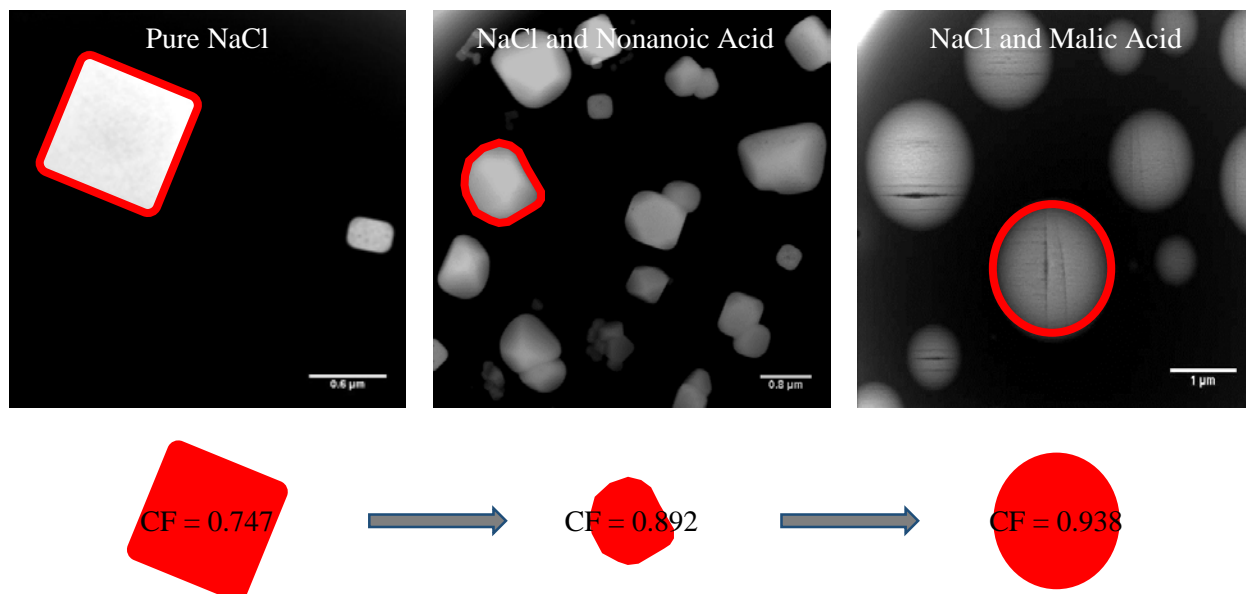
Figure 2.7 Images of three different types of aerosols taken with the TEM-HAADF detector. A representative particle of the population is outlined in each image and the corresponding circularity factor, calculated from ImageJ results, is shown below.

circularity factor is on a scale of 0.0-1.0, where 1.0 is a circle and 0.0 is an infinitely long straight line. As shown in Table 2.2, a perfect square will give a circularity factor of 0.785.

Applying this analysis to the particles studied, Figure 2.7 demonstrated the progression of reacted particles, from a square to a circle. Pure NaCl solutions generate the normal square shape that is associated with ionic salts, which has very little chloride depletion. Using the ImageJ program, this shape gives a circularity factor of 0.747. Progressing to a reaction between nonanoic acid and NaCl, which produces particles with ~20% chloride loss when compared to pure salt, images show aerosols that have a roundness to them, as well as some straight edges. The outlined particle produces a circularity of 0.892, which is neither a square nor a circle, but somewhere in between, as expected. Lastly, NaCl and malic acid particles are shown in the far right image. The particles that have essentially no chloride contained within the particle appear to be very circular, producing a circularity factor of 0.938. From this it can be concluded that, assuming no other processes occur, chloride depletion can be tracked by using the circularity factor. As a particle loses chlorine to the production of HCl (g) upon formation of the aerosol particle, the collected

19

aerosol will lose its crystalline square shape associated with pure NaCl and become progressively more spherical. However, this measurement does have some draw backs. First, the circularity factor is a two-dimensional analysis of a three dimensional object. Secondly, Eq. (2.2) does not take into account elongation of the particles, which is why particles with an ellipse shape or a rectangular shape can produce the same circularity factor. Images should be shown alongside any analysis involving circularity factor. More studies on how to include elongation into the circularity factor could be done. Lastly, the limitations of pixel sizes of ImageJ plays a role in shifting the calculated circularity factors, as can be seen in the circularity factor reported in Figure 2.7. The program takes into account the perimeter of each jagged pixel on the edge, creating a longer reported perimeter than should actually be. This is especially true for aerosols that have curved edges. The longer perimeter causes the circularity factor to be reported lower than should be, exhibited by the reported CF of 0.938 for a nearly perfect circular particle. While there are imperfections, this method is a step forward in the quantifying the morphology of particles.

2.3 Conclusion

The similarities in Figures 2.4, 2.5, and 2.6 indicate that there is a limit of depletion for long chained fatty acids, around 20-25%, and the reaction will go to completion almost every time. This could be due to the fatty acids remaining on the surface of the nascent aerosol and only reacting with the NaCl components near the surface, whereas more soluble acids, such as malic acid, are more likely to react with NaCl molecules throughout the newly formed aerosols, releasing more HCl (g). It appears that there is somewhat of a cutoff for hydrochloric acid displacement in terms of fatty acid carbon chain length. The three acids with long carbon chains, C-6, C-9, and C-16, all produce similar results, while C-4 malic acid produces much lower depletion levels. However, this could also be more due to the mono vs. dicarboxylic properties of the acids. A follow

20

up experiment using acetic acid (C-2, monocarboxylic), butyric acid (C-4, monocarboxylic) and succinic acid (C-4, dicarboxylic) would further our understanding. Regardless, it is evident that commonly found ocean surfactants can lead to depletion in chloride to sodium levels of nascent aerosols, which is suggested here, can occur upon the formation of the aerosol particle, in addition to the heterogeneous reactions of aerosols with SOA in the atmosphere. The changes in chloride levels reported here may have an impact on the viscosity, hygroscopic properties, and the cloud condensation/ice nuclei capabilities of the particles [Laskin et al., 2012]. The results from this chapter help lay the foundation of the hypothesis stated and show that it could be possible. The findings from the following chapter, Chapter 3, will help prove this hypothesis.

CHAPTER 3 – IMPACTS BIOLOGICAL BLOOM EXPERIMENT

Under the right conditions, which includes an abundance of nutrients, moderate temperatures, and light, algae can rapidly grow into what is known as a bloom. Algae blooms occur all over the world, in fresh and sea water, depending on the time of the year [EPA, 2013]. When a bloom occurs, it often only consists of one or a small number of phytoplankton species that are involved. When phytoplankton blooms occur in the ocean, they often cover a large surface area of the ocean. This will affect the chemistry of the ocean environment and will affect what gets released into the atmosphere, therefore affecting the weather and climate of the areas around and downwind of the algal bloom [Diersing, 2009]. Shown in Figure 3.1 is the global scale on which aerosols are transported [Putman, 2012]. The simulated image shows the far reaching capabilities of atmospheric aerosols, including sea spray (shown in light blue). Creamean et al. [2013] provide evidence suggesting that Saharan sand atmospheric aerosols impact the weather precipitation on the Western coast of the United States. While sea spray aerosols are not directly discussed within this context, it is proof of the importance of aerosol study and the impacts they can have on the weather and climate, even half way around the world!

What is unknown about these blooms is how they affect the transfer of chemical and biological species from seawater surfaces to the atmosphere via sea spray aerosol particles. In this chapter, the effects of a controlled phytoplankton bloom on the chemical composition of sea spray aerosols will be discussed and how those changes track throughout the birth, life, and death of the world's largest indoor biological bloom.

3.1 Investigation into Marine PArticle Chemistry and Transfer Science

In order to bridge the gap between laboratory and field settings, Prather et al. [2013] describe the use of a unique ocean-atmosphere facility, located in La Jolla, California at the Scripps

22
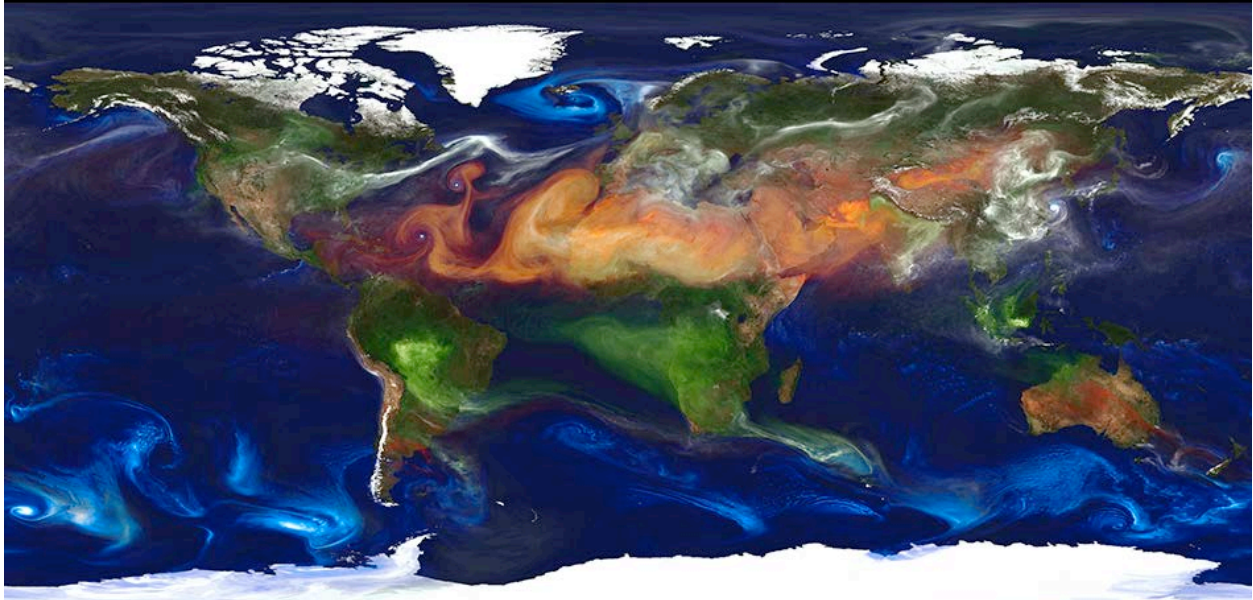
Figure 3.1 This portrait of global aerosols was produced by a GEOS-5 simulation at a 10-kilometer resolution. Dust (red) is lifted from the surface, sea salt (blue) swirls inside cyclones, smoke (green) rises from fires, and sulfate particles (white) stream from volcanoes and fossil fuel emissions. (Public domain image credit to William Putman of NASA/Goddard).

Institution of Oceanography, which can produce breaking waves with seawater, replicating natural marine settings, in the absence of background particles. This newly developed waveflume approach can reproduce the chemical complexity of the ocean, allowing for many mesocosm experiments to be conducted. The 33 m long flume can be filled with fresh sea water from directly from the ocean and spiked with nutrients to grow biological microorganisms, which can then simulate conditions all around the world. This system is able to produce sea spray aerosol particles for online and offline analysis and is critical for the development of our understanding of the way that sea spray aerosols impact the global climate [Prather et al., 2013]. The experiments was called IMPACTS for "Investigation into Marine PArticle Chemistry and Transfer Science".

3.1.1 Experimental Setup

During the summer of 2014, members of CAICE gathered at the Scripps Institute of Oceanography to begin the world's largest indoor phytoplankton bloom. From June through August, over 40 researchers from seven institutions conducted an experiment to measure the

www.manaraa.com

composition and chemistry occurring in sea spray particles could be researched in a controlled laboratory environment. Through a variety of online (such as aerosol time of flight mass spectrometer (ATOFMS), chemical ionization time of flight mass spectrometer (CITOFMS), and cavity ring down spectroscopy) and offline (including scanning electron microscopy (SEM), transmission electron microscopy (TEM), Raman spectroscopy, and atomic force microscopy (AFM)) techniques, the resulting aerosols were able to be studied. The exact details of this experiment and setup of all techniques not pertinent to this research, can be found elsewhere [Wang et al., 2015], but a brief summary will be given.

3.1.1.1 Wave Channel

Seawater was collected 5 m below the surface of the ocean from the Scripps Pier in La Jolla, CA and transferred into the 33 m wave flume at the Scripps Institute of Oceanography. Once filled, the tank was spiked with f/2 algae growth medium (Proline, Aquatic Eco-Systems, Apopka, FL) in addition to solutions of sodium metasilicate. The wave channel was continuously illuminated for the length of the experiment using 5700 K full spectrum lights. A wooden paddle was used to generate breaking waves within the flume. The waves were generated for 3 hours at a time, in order to ensure the continued growth of the phytoplankton bloom, as too much plunging can cause a premature death.

3.1.1.2 Sample Deposition

Similar to the discussion presented in Chapter 2 about particle deposition, the generated nascent sea spray aerosol particles were collected via a Micro-Orifice Uniform Deposition Impactor (MOUDI, MSP Corp. Model 110). The inlet tube for transfer of sea spray aerosols to the MOUDI was placed approximately 4 m from the point of wave breaking. Individual particles were collected on the sixth stage of impactor, with aerodynamic diameters between 0.56 and 1 μm.

24

Date	# of Particles Analyzed
July 7th	375
July 13th	426
July 17th	390
July 19th	398
July 21st	230
July 25th	313
July 29th	324
Total	2456

Table 3.1 Tabulated number of particles examined by CC-SEM/EDX on each day analyzed.

Samples were collected on copper TEM grids (Ted Pella, Inc.) for computer controlled scanning electron microscopy analysis (CC-SEM) and transmission electron microscopy (TEM) analysis. Additionally, particles were collected on quartz discs (Ted Pella, Inc.) for micro-Raman spectrochemical analysis.

3.1.1.3 CC-SEM with Energy Dispersive X-ray Spectroscopy

For single particle analysis, a Hitachi S-3400 Scanning Electron Microscope was used for imaging particles deposited on a TEM grid. The electron beam was set at an accelerating voltage of 15 kV and a current of 15 μA. A working distance of ~9.5 mm and a magnification of x10k were also used. All other settings were kept at default. The energy dispersive x-ray detector (IXRF Systems, Inc.) allowed for the collection of an excitation spectrum of elements contained within or around singular particles. Spectrum were collected for 20 s, to ensure enough counts and sufficient signal to noise. The EDX software, Iridium Ultra (IXRF Systems, Inc.), was used to set up an automated computer analysis. The computer controlled analysis is set up so that the program images the current field of view, measures all particles, and creates a black and white mask to distinguish between particle and substrate. The program will collect a spectrum from each particle within the view and, once completed, move on to the next field to repeat the process. The elements

25
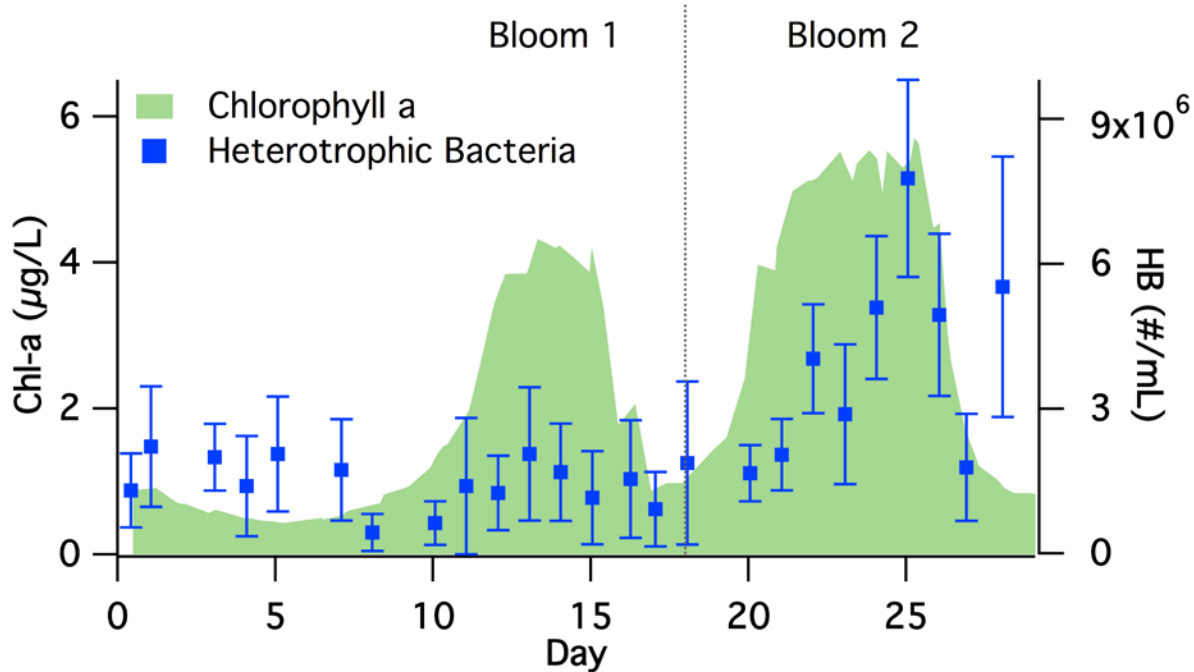
Figure 3.2 ESP chlorophyll count for the IMPACTS summer 2014 intensive experiment is tracked in green. (Data is credited to Jon Trueblood and Camille Sultana). The red is heterotrophic bacteria count data. Day 0 corresponds to July 3rd, 2014. (Data is credited to Francesca Malfatti). (Figure credited to Camille Sultana).

considered in the X-ray analysis were C, N, O, Na, Mg, P, S, Cl, K, and Ca. The resulting analysis is imported into a Microsoft Excel spreadsheet and analyzed. Table 3.1 includes the number of particles analyzed using CC-SEM per day.

3.1.2 Results and Discussion

In order to track the progression of the bloom, the chlorophyll-a was tracked during the length of the IMPACTS campaign. Chlorophyll-a has commonly been a method used by researchers to track the health and activity of algal blooms [Boyer et al., 2008]. Chlorophyll-a is an indicator of phytoplankton biomass because all phytoplankton contain chlorophyll-a, as it is necessary for the method the organisms use for photosynthesis process, in order to create energy [Czuba et al., 2011]. Phytoplankton can be divided into two classes, algae and cyanobacteria. As both classes need light to photosynthesize, phytoplankton in any environment, fresh or saltwater, will float near the top of the water, where sunlight reaches. Therefore, there are numerous ways

26

that ways that phytoplankton affect the components of sea spray aerosols. First, marine phytoplankton are known to excrete many different organic compounds directly into ocean water, as a mechanism to remove metabolic wastes and as chemical communicants, among other potential reasons. These compounds can range from keytones and aldehydes to alcohols and fatty acids [Gagosian, 1981]. Often, these compounds, like fatty acids, will have nonpolar properties, causing them to rise and concentrate to the ocean surface. Secondly, biological organisms are made of numerous organic materials [Becker et al., 2014]. For example, one of the most common long chain fatty acid found in lipids (a component of biological membranes) of algae, is palmitic acid (16:0), which is highly insoluble in water [Baker, 2004]. When organisms die and decompose, the insoluble and hydrophobic cellular components will rise to the ocean's surface, concentrating in the seas surface microlayer [Adams et al., 2013]. This also is why often many fatty acids can be found in this region. Additionally, as Aller et al. [2004] point out, there have been reports that suggest bacteria counts can be 10^2-10^4 times higher in the sea surface microlayer than in the waters directly below. When aerosols form from bubble bursting, it is not unheard of for small diatoms or bacteria to reach the aerosol phase [Aller et al., 2004].

Figure 3.2 shows the results of the nutrient addition at the beginning of the IMPACTS experiment to initiate phytoplankton growth. Tracked using the fluorescence of the chlorophyll-a, two consecutive phytoplankton blooms occurred over a 29 day period. The first bloom occurred from July 11th to July 20th, peaking around the 16th/17th of July. Interestingly, the heterotrophic bacteria count, measured via epifluorescence microscopy, stayed around the normal levels. In contrast, the second, more intense bloom occurred from the 23rd to the 31st, peaking from the 24th until the 28th, showed increased levels of bacteria. The possible explanations for this trend are found in Wang et al. [2015].

27
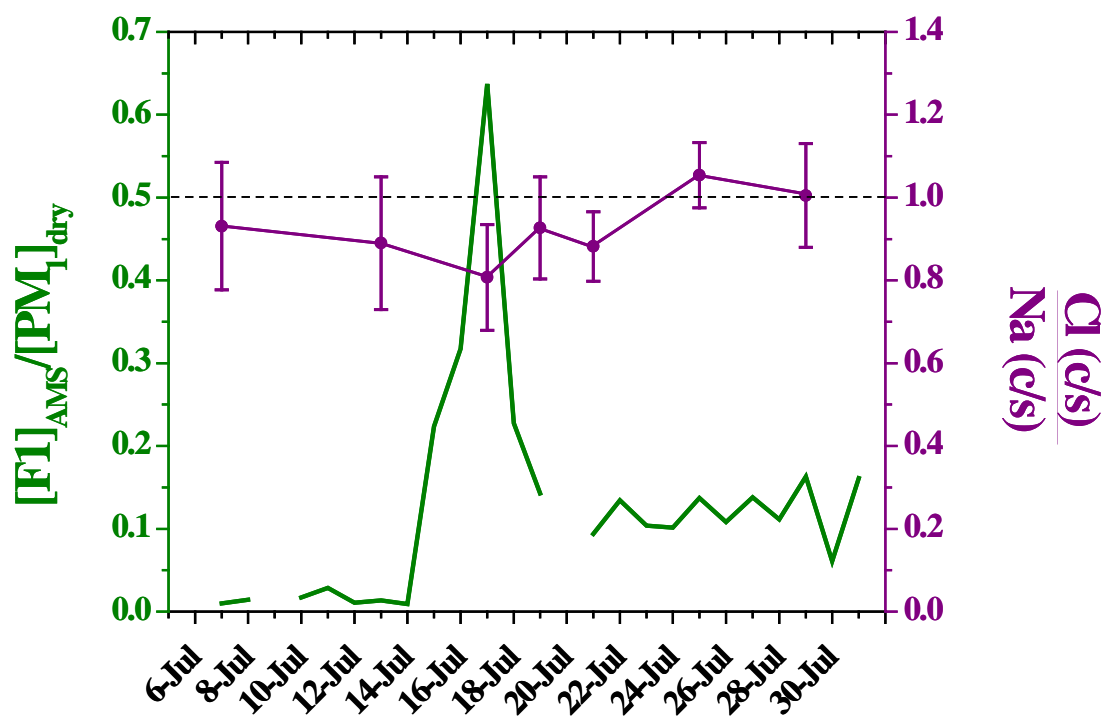
Figure 3.3 The Cl/Na ratios of every particle analyzed for each day of interest with the CC-SEM was fit to a Gaussian curve. The averages are plotted in purple, with the standard deviation represented by the error bars. The ratios are plotted against the measured $[F1]_{AMS}/[PM_1]_{dry}$ (green), which signifies the amount of aliphatic-rich particles (low O:C ratios) normalized to the concentration of sub-micron particles produced. The dashed black line represents the Cl:Na ratio of unreacted NaCl. (AMS data collected by Xiaofei Wang).

Building off of the discussion in Chapter 2, Figure 3.3 provides a major finding for the chemical components of the sea spray particles. After thousands of spectra were collected using the CC-SEM, the Cl/Na signal ratios were analyzed. Figure 3.3 demonstrates the significant decrease of chlorine in particles on the 17th of July, which happens to be correlate with the apex of the first chlorophyll-a peak. The ratio, which is slightly more than 0.8 Cl/Na, is much lower than any of the surrounding days analyzed. Corresponding with this drop in chlorine levels is a considerable increase in the concentration of particles with aliphatic-rich (compounds with low O:C ratios) signal normalized to the concentration of sub-micron particles signal detected within the aerosol phase by the Aerodyne Aerosol Mass Spectrometer (AMS). Consequently, this suggests that organics are being transported into the aerosol phase and upon formation, are reacting

with the NaCl, displacing the Cl anion to form $HCl_{(g)}$ and the corresponding salt. This trend is similar to what is seen in the model experiments conducted and reported in Chapter 2, above. While Laskin et al. [2012] have pointed to this acid displacement as a byproduct of heterogeneous reactivity between secondary organic aerosols (SOA) and sea spray, there are no SOAs capable of reacting with the nascent aerosols in this experiment. This fact instead points to the probability that the chlorine depletion occurs even before the aerosol has fully formed. While this work is not to disprove the work suggesting that some chlorine depletion can occur during atmospheric reactions with SOAs, but it does show that chlorine depletion can be affected by the components of the sea water it results from.

Furthermore, Figure 3.3 also exhibits a Cl/Na ratio close to 1/1 on July 25th and 29th, right during the peak of the second blooming period. There could be a few different reasons for this trend. This could mean there are much fewer organics on the ocean surface that are able to get to the aerosol phase, which is supported by the steep drop in the concentration of aliphatic-rich particles detected by the AMS after the 17th. This could be due to the slowing of the production of aliphatic organic excrement by the heterotrophic bacteria/phytoplankton. While the total counts of the bacteria and phytoplankton are at increased levels during this period, the biologicals could be producing more oxygenated compounds, thus promoting a separate reaction upon formation than the aliphatic-rich compounds had. Alternatively, the production of organics by the organisms could have shifted to a more hydrophilic short chained organic compounds. This would cause the selectivity of the organic components of the water to shift towards wanting to stay in the bulk solution and not being entrapped by the formation of the sea spray aerosol. There is evidence supporting the production of short chained organics during the second bloom reported in the Wang et al. paper [2015]. Lastly, while still at elevated levels of live bacteria, a significant amount of
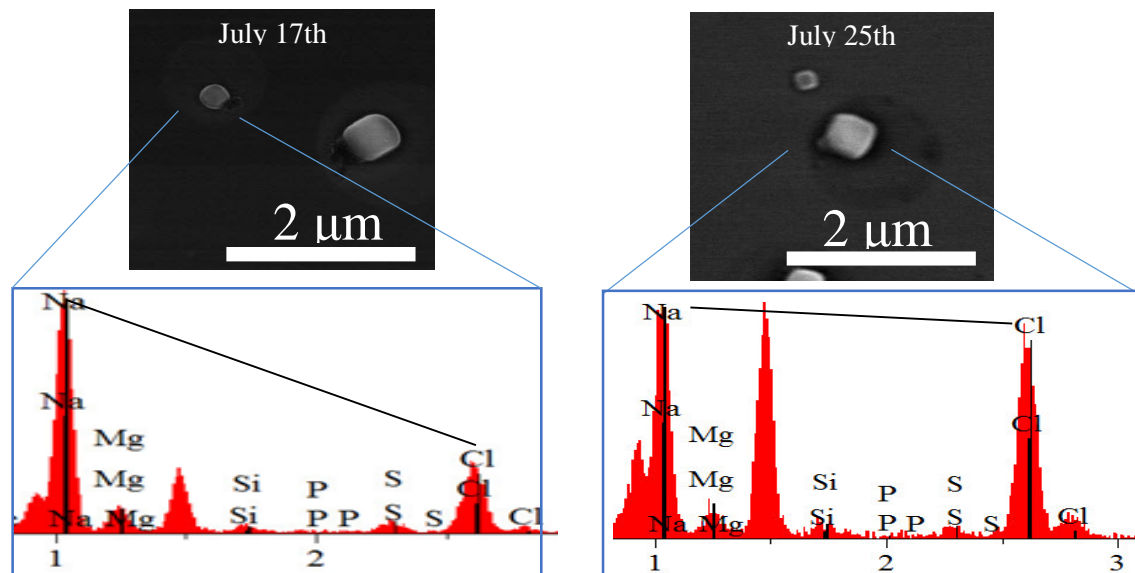
Figure 3.4 Example spectra of particles from the two different blooming periods. The particle from July 17th shows a significant drop in chloride levels when compared to the particle from the 25th. The large marked (*) peaks are the Al Kα peak, which is generated from the substrate holder.

bacteria could have died off at this point in the bloom. This would increase the levels of long chained fatty acids in the water due to the decomposition of the bacteria walls. Since fatty acids are extremely hydrophobic and insoluble, they will be concentrated at the air-water interface, and therefore more likely to be entrapped upon the formation of the sea spray aerosol. For example, palmitic acid would be in high abundance, as it is a component of phospholipids found in cell membranes [Schenkel et al., 2014]. Shown in Chapter 2, the overall effects of long chained, insoluble fatty acids do not tend to displace the chlorine in sodium salt particles. Further research will need to be conducted in order to conclude which explanation is the most viable.

Figure 3.4 provides two example spectra from the CC-SEM analysis. The image on the left, which gives a calculated 0.91 circularity factor, provides a spectrum that has over 50% chlorine depletion, when compared to the expected 1/1 ratio. This shows evidence that particles have reacted with organics and significant acid displacement has occurred. The second image of a particle on the 25th, during the second blooming period, gives off a spectrum of near 1/1 ratio,
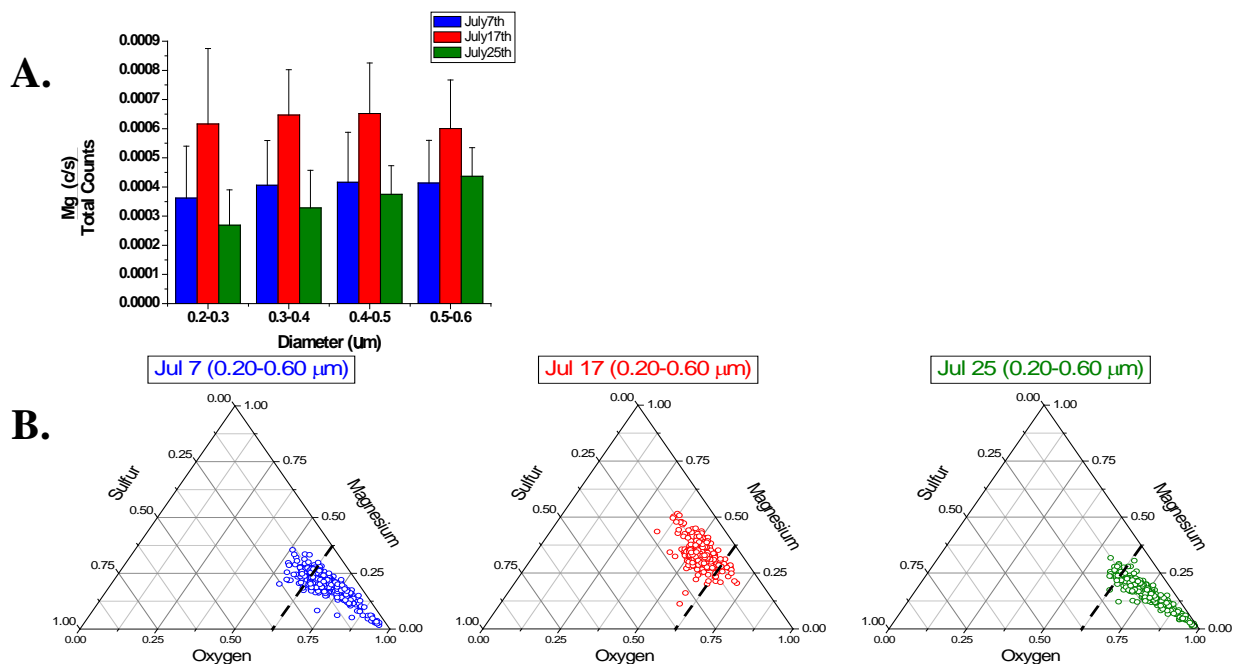
Figure 3.5 These figures demonstrate the relative amounts of magnesium contained within the SSA. As seen, the Mg2+ levels are elevated on July 17th, the same day as the high AMS ratio and the high Cl- depletion. The dotted lines are only to make it easier to see trends and have no other significance.

which is expected of unreacted, pristine particles. The particle also give a circularity factor of 0.81. This also lends evidence to the hypothesis, laid out in Chapter 2, that particles can become more spherical with chloride loss.

Figure 3.5 shift the focus to the levels of magnesium contained within the particles collected. For visual purposes, the days of focus were the pre bloom (July 7th), the height of the first bloom (July 17th), and the peak of the second bloom (July 25th). Part A shows the average total magnesium counts normalized to the total counts per particle per day in each size bin. The value of the error bars is plus/minus one standard deviation. On the same day as the peak of the AMS ratio, shown in Figure 3.3, there is also a peak increase in magnesium, when compared to the other two days. The divalent cation magnesium has long been associated with biological activity seen in ocean water. Magnesium is a coordinating ion in the chlorophyll molecule, which can be found in cyanobacteria and algae. The cation is also found in cell membranes and walls of

31

www.manaraa.com

biologicals. Demonstrated by the figure, the magnesium enriched matter is reaching the aerosol phase. However, this is not the case for the peak of the second bloom (July 25th), thus continuing the trends that are showing the two blooms are different. It is also interesting to note that on both the 7th and the 25th, the relative Mg^{2+} levels increase with increasing diameter, but the 17th is approximately constant for all measured size ranges. Figure 3.5B further emphasizes the shift in magnesium levels by using tertiary plots. The tertiary plots show that the average magnesium levels almost double on the 17th of July compared to the other two dates when plotted against sulfur and oxygen. We have attributed to the presence of Mg^{2+} to the formation of $MgSO_4$ on the particle [Ault et al., 2013]. However, as the magnesium levels increased on the 17th relative to sulfur and oxygen, there must be another source of Mg^{2+} contained within the particles. A possible explanation could be found in previous work, where it has been shown that the anionic nature of marine organic matter is bridged together by divalent cations to drive a polymer gel coalescence [Wells, 1998]. In IMPACTS, when the phytoplankton bloom reached its peak, there was more marine organic matter, which would attract more divalent cations, specifically Mg^{2+}. When aerosolized with chloride depleted NaCl, gels are able to form around the salt core, explaining the trends seen in Figure 3.5.

Through the data presented here, it has been established that particles can become chloride depleted via organic ocean surfactants upon the formation of the sea spray aerosol particle. While the exact reason why still needs to be uncovered, it is a critical finding that impacts the way SSA will interact within the atmosphere. Once the reason for the chlorine depletion is discovered, the resulting mechanism will need to be taken into account in aerosol models and how they impact the atmosphere.

CHAPTER 4 – METHOD DEVELOPMENT

Field experiments have been conducted all over the world on atmospheric aerosol particles, ranging from the Arctic to the Antarctic, the Pacific to the Atlantic, but no matter how desolate the area or how far it is off the shoreline, there is no way of knowing for certain whether or not the samples collected during these experiments contain contaminants from other far away aerosol sources. Additional questions have arisen about samples that have been stored for long periods of times or analyzed in vacuum chambers. These questions have led to the opportunity to pioneer and further develop aerosol collection, storage, and analysis techniques and protocols. This chapter will discuss the different methods that were developed over the past few years that has helped understand as well as bridge the gap between the laboratory studies and field measurements of sea spray aerosol.

4.1 Aerosol Generation Method Intercomparison

In nature, sea spray aerosol can be generated through different pathways. From waves crashing on the beach, to bubbles from the ocean floor bursting upon reaching the surface, to strong winds picking up the top layer of water and throwing it into the air [Grythe et al., 2014]. However, the sea spray aerosol natural generation mechanisms have been relatively difficult to replicate within the laboratory setting [Prather et al., 2013]. One of the most commonly used techniques, termed the sintered glass filter (SGF) technique, involves simply flowing air through a sintered glass filter and allowing the rising bubbles to burst and generate aerosols to be collected [Collins et al., 2014]. A schematic of the sintered glass filter technique is shown in Figure 4.1 [Keene et al., 2007]. Even though this method is widely used in the study of aerosol generation, these techniques do not replicate the complexity of generation mechanisms of natural sea spray aerosols from the oceans and recent reports have indicated that this atomization does not produce aerosols

33
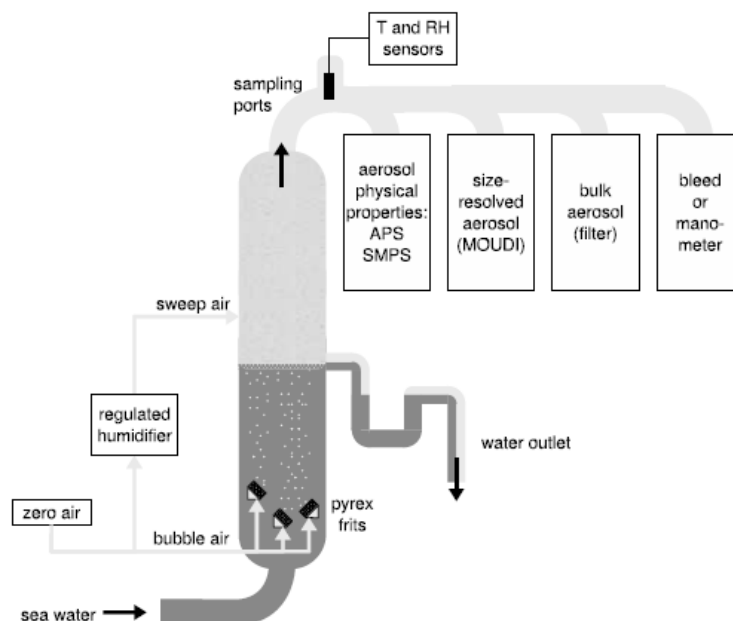
Figure 4.1. Schematic diagram of a typical sintered glass filter aerosol generation method. (Figure taken with permission from Keene et al., 2007).

with the same physical and chemical properties as natural methods [Gaston et al., 2011]. Therefore, in order to study these aerosols without any background particles/contaminants in the appropriate setting, researchers have had to literally bring the ocean into the laboratory [Prather et al., 2013]. In November 2011, Prather et al. (2013) were able to successfully introduce a unique ocean-atmosphere facility with authentic sea spray aerosol generation from natural ocean water by means of wave breaking in the laboratory setting. With this experiment, Prather et al. were able to show that they could produce aerosols that compare positively to those previously seen in field experiments [Deane et al., 2002]. While not all factors of the sea spray production were the same, it was a large step taken in the closing of the environmental/laboratory gap.

One major drawback to this experiment was that it was done at the Scripps Institute of Oceanography (SIO), located in La Jolla, CA, in a waveflume channel, the schematic of which is shown in Figure 4.2, that measures approximately 33 meters in length and can hold over 11,000 liters of fresh sea water pumped directly from the Pacific Ocean. While this facility is open to

34
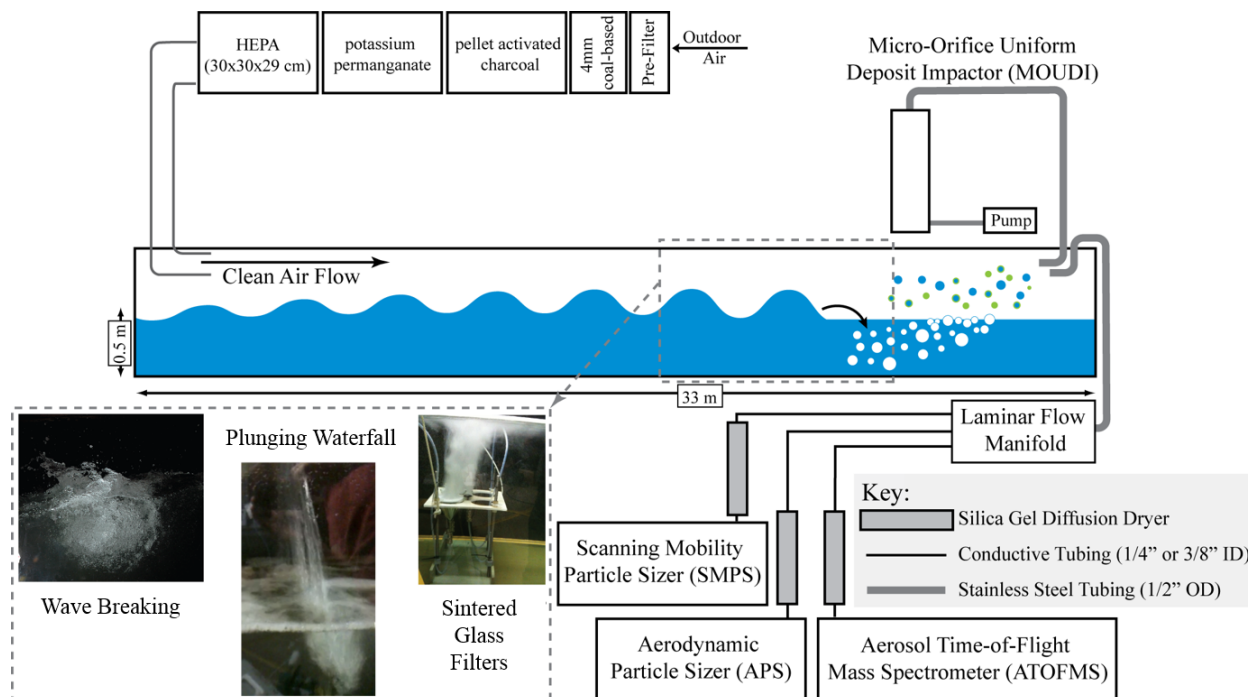
Figure 4.2. Schematic of the linear wave channel with interchangeable bubble generation apparatuses for SSA production. (Figure taken from Collins et al., 2014).

outside users, it is not practical for most researchers to be to replicate this new gold standard in laboratory sea spray generation. Therefore, the marine aerosol reference tank (MART) was developed by the researchers at the Scripps Institute and University of California-San Diego (UCSD), shown in Figure 4.3. This scaled down version of the waveflume is much more efficient for research labs to conduct their own experiments generating sea spray aerosols [Stokes et al., 2013]. As Stokes et al. showed, the waterfall plunging method of aerosol generation used in the MART system, is very comparable to sea spray generated via the wave breaking method, in terms of bubble size distribution and number concentration of particle diameters, and both differ greatly from the popular sintered glass filter method. However, a study of the size, morphology, and chemical composition of the resultant aerosols of these techniques needed to be done in order to determine if the techniques in question are producing aerosols with comparable shape and elemental composition to those produced by the wave breaking action of the ocean or wave-flume.
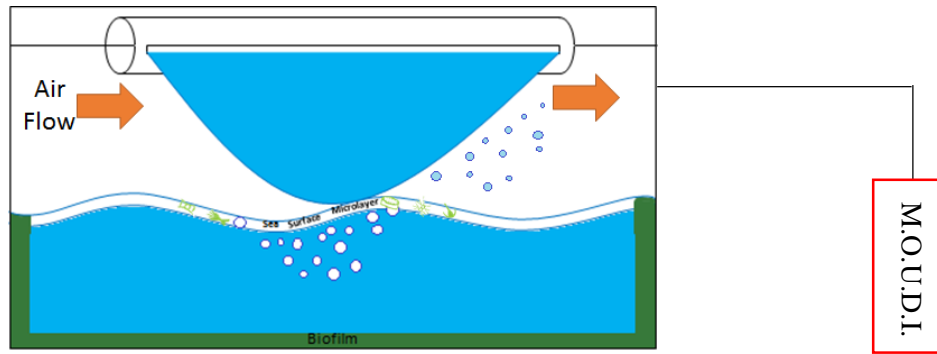
Figure 4.3. A simple schematic of the Marine Aerosol Reference Tank (MART).

4.1.1 Experimental Setup

Collins et al. [2014] provides the experimental setup description in full, but the following is a brief description of the experimental procedure done by Doug Collins at the University of California, San Diego.

4.1.1.1 Sea Spray Aerosol Generation Methods

The wave flume described in Prather et al. [2013] was the system used to generate samples for this comparison analysis, a schematic of which is shown in Figure 4.2. The flume was filled with water collected off the Scripps Institute of Oceanography Pier before each experiment. There were three different aerosol generation techniques tested for this experiment: controlled wave breaking, plunging waterfall, and sintered glass filters. One sample of aerosols was generated by breaking waves, created by a hydraulic paddle within the waveflume. Another sample was generated by a plunging waterfall, where recirculated seawater is pumped to a horizontal slotted cylinder approximately 40 cm about the water surface [Collins et al., 2014]. The water plunges to the surface in repeated spurts, generating aerosols. The final method of sample generation produces aerosols by forcing nitrogen gas through two sintered glass filters located 35 cm below the water's surface, creating bubbles that burst upon surfacing, creating the sea spray of interest.

www.manaraa.com

4.1.1.2 Sea Spray Aerosol Collection Method

Aerosol samples generated from the above methods were deposited on silicon wafer substrates using a micro-orifice uniform deposit impactor (MOUDI) (MSP Corporation). Aerosol samples were collected on stages 4-8 of the MOUDI, each with its own diameter size ranges, which can be found elsewhere [Ault et al., 2013]. For the analysis done in this experiment, the stage 6 sample was used, which collects particles with an aerodynamic diameter size range of 0.56-1.0 μm. Particles were deposited wet at ~90% RH and stored at The University of Iowa at ~20% RH.

4.1.1.3 Sample Analysis

The samples collected during this experiment were analyzed here at the University of Iowa, using a scanning electron microscope (SEM) for images, allowing for size and morphology analysis. The SEM is also coupled with an energy dispersive x-ray spectroscopy (EDX) system, which can acquires an x-ray spectrum from the deposited aerosols. SEM images were collected using a Hitachi S-4800 scanning electron microscope. The images were taken using a secondary electron detector and the adjusted settings were set at an accelerating voltage of 5 kV, beam current of 15 μA, x10k magnification, and a working distance of ~9.5 mm. All other setting were kept at default. Spectra were taken using the Integrated X-Ray Fluorescence (IXRF) Systems, Inc. energy dispersive x-ray spectroscopy elemental analysis system. Single particles analysis was performed using a computer controlled SEM (CC-SEM) program, Iridium Ultra (IXRF Systems, Inc.), which allows for automated EDX analysis of thousands of particles. The software identifies particles in a particular field of view on the substrate, acquires a spectrum for 20 s at the SEM settings already described, and moves to the next particle. Once all of the particles in one field have been analyzed, the program will move the sample stage to the next field, and the process repeats itself until the predetermined time limit had expired. The software automatically determines the area of each

37

dPA (μm)	Wave Breaking	Plunging Waterfall	Sintered Glass Filters
0.3–0.4	54	171	166
0.4–0.5	41	75	76
0.5–0.6	37	42	29
0.6–0.7	31	37	17
0.7–0.8	28	49	13
0.8–0.9	32	48	38
0.9–1.0	27	29	31
1.0–1.1	28	38	35
1.1–1.2	25	29	25
1.2–1.3	22	41	20
1.3-1.4	26	44	14
1.4–1.5	30	45	11
1.5–1.7	45	59	16
1.7–1.9	27	62	33
1.9–2.1	33	52	26
2.1–2.3	17	36	20
2.3–2.5	13	19	18
2.5–2.7	9	13	23
2.7–3.0	6	5	17
Total	**531**	**894**	**628**

Table 4.1 Tabulated number of particles analyzed by CC-SEM/EDX in each size bin for the three different aerosol generation methods used to generate sea spray aerosol.

particle detected by the program. The area was used to calculate projected-area diameter (dPA) using Eq. (2.1):

$$d_{PA} = \left(\frac{4A}{\pi}\right)^{1/2} \tag{2.1}$$

where A is the area of the particle detected by the Iridium Ultra software. Each particle was placed into a size bin, dependent on their d_{PA}. Table 4.1 lists the number of particles analyzed in each size bin for each aerosol generation method. Images from the SEM technique were also used to determine the circularity factor of particles, using Eq. (2.2):

$$C = \frac{4\pi A}{P^2} \tag{2.2}$$

where A is the area of the particle and P is its perimeter calculated using the software program ImageJ.

38

4.1.2 Results and Discussion

After using the CC-SEM/EDX to analyze over 2000 particles, we were able to do semi-quantitative chemical analysis of these particles. In order to keep the background substrate silicon peak from overwhelming the signal of all of the elements of interest, the SEM was set at an accelerating voltage of only 5 kV. This is not enough voltage to fully excite all of the excitations of each element of interest contained within the particles, but it is enough to give an elemental peak if that element is present. In order to make semi-quantitative conclusions, we looked at the relative intensities in the counts per second of the cations of interest, specifically Mg^{2+}, K^+, and Ca^{2+} with respect to the counts per second of Na^+. In doing this, we were able to make conclusions about the relative quantities of these elements. This allows us to overcome any dependence of the elemental spectral signal on the size of the particle [Laskin et al., 2006] and on the accelerating voltage [Willis et al., 2002].

The results of this analysis are shown in Figure 4.4. Furthermore, the figure is presented in a way that everything is relative to the elemental ratios measured in the particles collected from the wave breaking (WB) method, often considered the "gold standard" for laboratory sea spray aerosol generation. Figure 4.4a shows the average signal ratio of X/Na (X = Mg, K, and Ca) for SSA in that size bin generated from the plunging waterfall (PW) method, divided by the average signal ratio of X/Na for SSA in that size bin generated from the wave breaking method. Figure 4.4b shows the exact same thing, except the particle were generated by the sintered glass filter (SGF) method instead of plunging waterfall. Particles that have no difference in X/Na ratio in the SSA produced by the methods being compared give a value of one, shown in the figure by the solid black line. Therefore, the closer the average ratio is to 1, the more similar the aerosols being compared. As Figure 4.4a shows, the chemical composition of the aerosols created by PW and
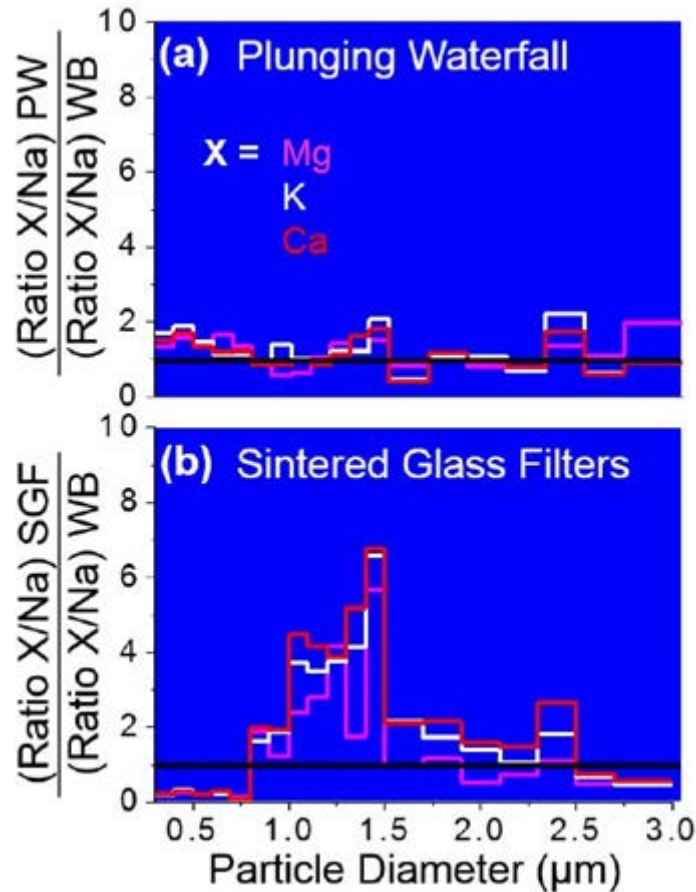
Figure 4.4 Elemental composition of particles produced via a.) plunging waterfall and b.) sintered glass filters, compared to particles produced via wave breaking. The comparison is made using the ratio of the EDX intensities (counts per second) for Mg, K, and Ca referenced to Na in individual SSA particles. The solid black line indicates a 1:1 ratio between plunging waterfall or sintered glass filters to wave breaking. (Figure taken from Collins et al., 2014).

WB are very similar throughout all size ranges for all cations, rarely going outside the ratio range of 0.5-2. In contrast, the aerosols generated by the SGF method show considerable difference when compared to those of WB. At lower size ranges, the Mg/Na, K/Na, and Ca/Na signal of SGF particles are suppressed, well below ratio levels of 0.5. The greatest difference between the two graphs occurs in the 1.0-2.0 μm range where SGF ratios spike to over 7 fold that of the WB ratios. This indicates a large enrichment of non-Na$^+$ cations in super-micron particles. Additionally, the particles in the 0.3-0.8 μm range are generated with suppressed levels of non-Na$^+$ cations, all of which could alter the particles physicochemical properties.

40
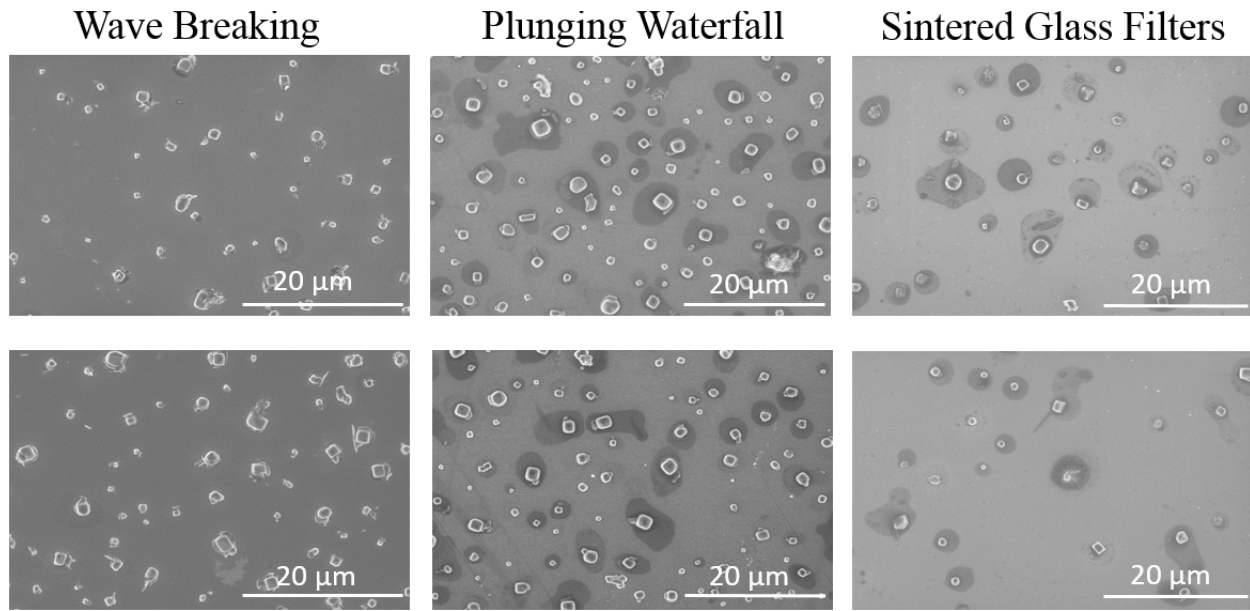
Figure 4.5 SEM images taken of samples from three different aerosol generation methods, demonstrating the drastic difference between (Figure taken from Collins et al., 2014).

These results emphasize the importance of single-particle analysis and the need for size resolved data. The elemental compositional findings of the CC-SEM/EDX experiment in the super-micron particle range are in agreement with the aerosol time of flight mass spectrometry (ATOFMS) data reported by Collins et al. [2014], and supports the idea that, while the sintered glass filter method of sea spray aerosol generation was an adequate technique in the past, but our advancing capabilities need a more accurate method of SSA production, like the plunging-waterfall method.

Additionally, we investigated the morphology of the particles created by each method. Circularity factor is the measure of how closely a particle approaches that of a circle. A perfect circle would have the circularity of 1.0, where as a square would have a circularity of 0.79. Given in Table 2.2 is the circularity factor of many different shapes for reference. While not this factor is not always accurate due to elongation and particles with irregular edges, this statistic allows us to quantify morphology, as opposed to just concluding that something "looks rounder." To help compare between the three methods, the circularity parameter (defined in Eq. (2.2)) of nearly 100

41

particles with a d_{PA} between 0.38 and 2.6 μm from each method was measured using ImageJ software. Particles were classified as either spherical (C = 1.00±0.10) or cubic (C = 0.79±0.08) based on their circularity factor being within 10% of an ideal sphere or cube, respectively. The core crystals were the only part of the particle taken into account. Figure 4.5 shows examples images of particles from each generation method that was used for this analysis. As reported in Collins et al. [2014], it was determined that 56% of the sintered glass filter generated SSA particles measured were considered spherical, while only 44% of the plunging waterfall particles were classified as such. Though neither is as low as the 32% of particles from the wave breaking method, it is clear that the plunging waterfall particles are much more similar to those of the wave breaking than sintered glass filters. As discussed in previous chapters, the circularity of particles can be correlated to the amount of chloride lost to acid displacement due to reaction with organic acids. The significant increase in circular particles indicates that the use of sintered glass filters alters the selectivity of the aerosol during the generation process. By using this method, it is seen that it increases the amounts of organic reaching the aerosol phase, thus not being a true representative of actual sea spray aerosol particles.

While there are many other arguments and findings within the Collins et al. [2014] paper, we were able to show that there is a clear difference between all three methods, however, the plunging waterfall and wave breaking methods produce much more similar aerosols than those produced the sintered glass filter method. Therefore, future studies done in the laboratory setting on sea spray aerosol particles should be generated with the new plunging waterfall method, rather than the popular sintered glass filter method.

42

4.2 Storage Conditions

Another common practice in research pertaining to aerosols is to store samples in a freezer for weeks or even months before analyzing particles. The main reason behind this procedure is that if there are volatile components of an aerosol, these compounds will not evaporate in the freezing temperature. The idea is to keep the particles in pristine condition for as long as possible, as offline analysis sometimes cannot happen for months to even years after the initial collection date. However, there has never been a study to conclude that this approach is, indeed, the best storage method for aerosol samples.

For this study, three different techniques, optical microscopy (OM), atomic force microscopy (AFM), and scanning electron microscopy (SEM), were used to image particles collected during a MART experiment and particles collected from an aerosolizer, for a model system analysis comparison. The samples were collected and stored, for analysis, in two different conditions: freezer and ambient. The images acquired by aforementioned techniques were used to determine the size and morphology of the particles seen. The specific generation methods, sample collection, and OM and AFM procedures, as well as the results from OM and AFM techniques, can be found elsewhere [Laskina et al., Unpublished work]. The procedures and results in this section pertain to the SEM.

4.2.1 Experimental Setup

4.2.1.1 Sample Generation and Collection

Particles were generated during the two week phytoplankton bloom synthesized by Olga Laskina in collaboration with researchers at UCSD in a Marine Aerosol Reference Tank (MART) system during January 2014. The aerosols were generated using the plunging waterfall method examined in Section 4.1. The samples were collected using a MOUDI, depositing particles on

43

substrates on every stage, but stage 6 samples were used during this research. Particles collected on silicon wafers substrates were used for the SEM analysis. Once collected, one set of substrates was kept in a sealed petri dish stored in a cardboard box at ambient conditions, which were 17-23% RH and 19-21 °C. The second set of samples were stored in a sealed petri dish placed in a freezer at -12 °C. Before analysis, samples were allowed to equilibrate at room temperature for two hours.

Furthermore, aerosol samples were made from a solution of 0.1 M NaCl (Fisher Scientific, ≥99.0%) and malonic acid (Alfa Aesar, 99.0%) (2:1 NaCl to malonic acid molar ratio) using a constant output atomizer and dry deposited on silicon wafers attached to stage 6 of a MOUDI. Exactly like the samples collected during the MART experiments above, a sample was stored at ambient conditions and another sample was stored in a freezer. Additionally, a third sample was collected and stored in a desiccator at 0.2±0.1% RH. When getting prepared for SEM analysis, the desiccator and freezer samples were allowed to equilibrate at room temperature for approximately fifteen minutes and two hours, respectively. One sample was imaged and analyzed right after sampling, to provide a baseline for the experiments. After, each sample was imaged and analyzed at 3, 5, and 7 weeks after the initial sample collection date. NaCl/malonic acid solution generated particles were also collected on Quantomix QX-102 WETSEM capsules (of which are discussed further in Section 4.3), in order to image particles under atmospheric conditions while being in the vacuum chamber of the SEM. Comparisons to the particles exposed to the vacuum were made.

4.2.1.2 Sample Analysis

The research that is described here focuses on the SEM images, which were collected using a Hitachi S-4800 Scanning Electron Microscope, with a 5 kV accelerating voltage, a 5 μA beam current, and an 8 mm working distance for particles collected on silicon wafers. Images of particles
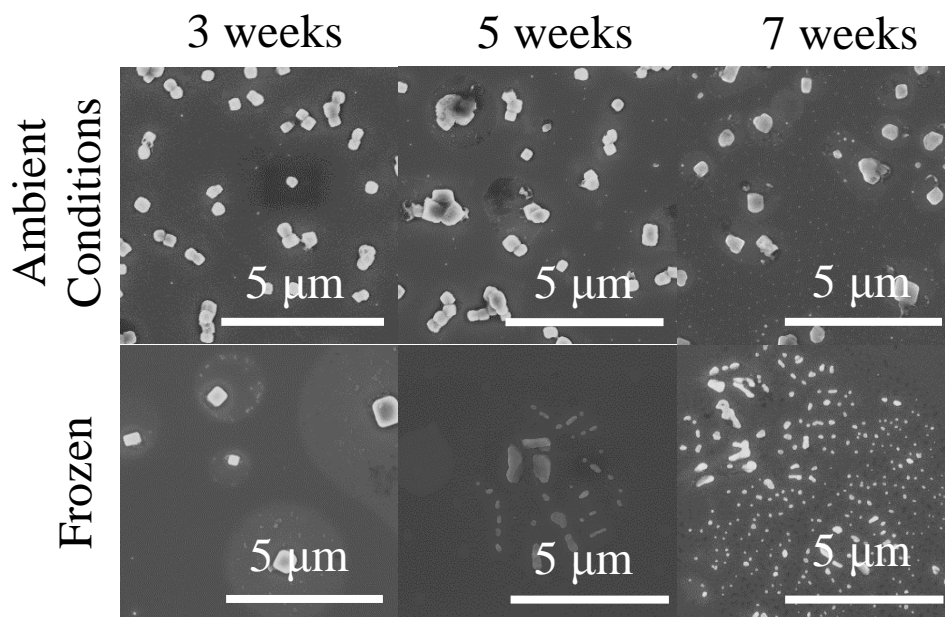
Figure 4.6 SEM images of SSA collected on silicon wafer substrates, taken at 3, 5, and 7 weeks after initial collection. (Figure adapted from Laskina et al., 2015).

in WETSEM capsules were taken at a 5 kV accelerating voltage, a 5 µA beam current, and a 10 mm working distance in order to compensate for the extra height of the capsule. Images were taken at a magnification of x10k for these experiments. Once the images were taken, they were analyzed in the same manner as described in Section 4.1.1.3.

4.2.2 Results and Discussion

The widely used process of storing aerosol samples in a freezer and subjecting the samples to multiple thawing and refreezing cycles assumed that there is no change in the chemical and physical state of the sample specimen. Figure 4.6 shows SEM images taken of samples collected in the January MART biological bloom experiment stored at two different conditions. The top row shows images of samples stored at ambient conditions. As can be seen, there does not appear to be a large or noticeable change in the size and morphology of the particles over time. On the contrary, the second row of images shows that particles stored in the freezer change over time, not only when compared to ambient storage conditions, but over the course of several weeks, as well. It

45
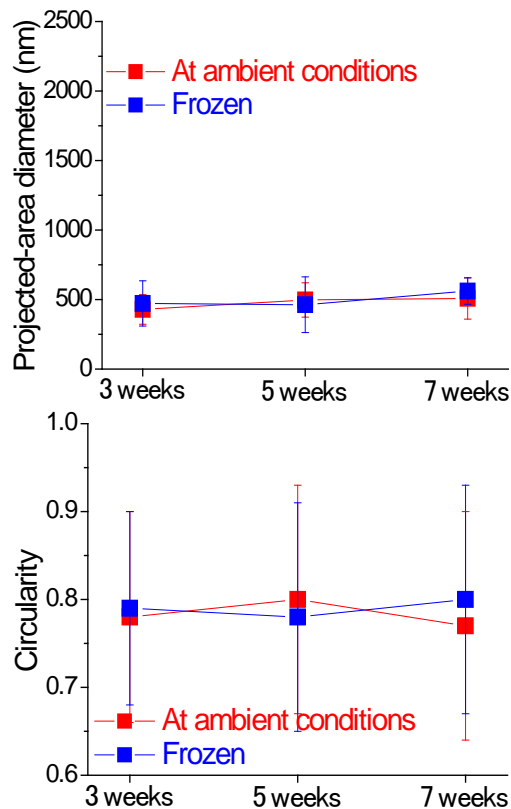
Figure 4.7 The projected-area diameter and circularity measured for all particles imaged using the SEM. As shown, there is little significant difference between the ambient conditions and frozen conditions. (Figure adapted from Laskina et al., 2015).

appears that the samples become more and more fractionated and some particles seem to become increasingly irregular in shape. However, when measured for diameter and circularity for quantitative analysis, the particles from both samples have nearly the same averages, certainly well within one standard deviation of each other, shown in Figure 4.7. This interesting trend is attributed to the fact that when the particles stored in the freezer are taken out to thaw and equilibrate, they take up water. Particles that are spatially close to each other will aggregate together. When entered into the vacuum chamber of the SEM, the particles will dehydrate back to approximately their original size, but upon efflorescence (drying out process from a liquid to a solid state), may reform the crystal structure to that of which is seen in the images of weeks 5 and 7 in Figure 4.6. As for

46
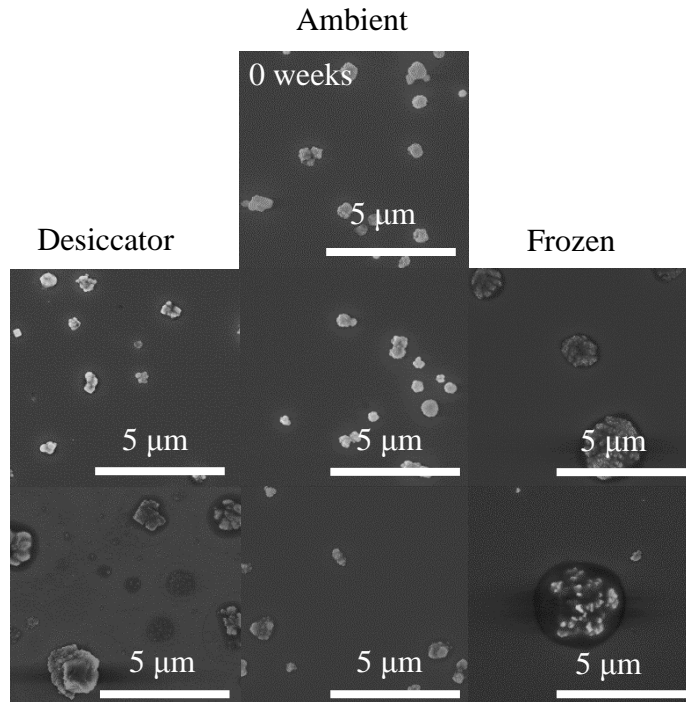
Figure 4.8 SEM images of aerosols generated from NaCl/malonic acid solution collected on silicon wafer substrates, taken at 0, 2, and 4 weeks after initial collection and stored in three different conditions. (Figure adapted from Laskina et al., 2015).

the change in morphology of these particles as measured by the circularity parameter, the values given in Table 2.1 show that a lot of different shapes can give about the same circularity factor and look completely different. Usually rounded, elongated particles and aggregated particles can throw off a circularity analysis of a population, of which both types of particles were commonly seen in this frozen sample. As a result of a combination of these reasons, Figure 4.7 shows little to no quantitative differences, unlike the images from Figure 4.6. While the SEM results on these samples were inconclusive by itself, when combined with the results from the Raman optical microscope (Olga Laskina) and the AFM (Holly Morris), we were able to show a significant increase in diameter of the particles stored in the freezer over the four weeks, but, in regards to circularity, were unable to show much of a difference, similar to the results of the SEM, discussed above.
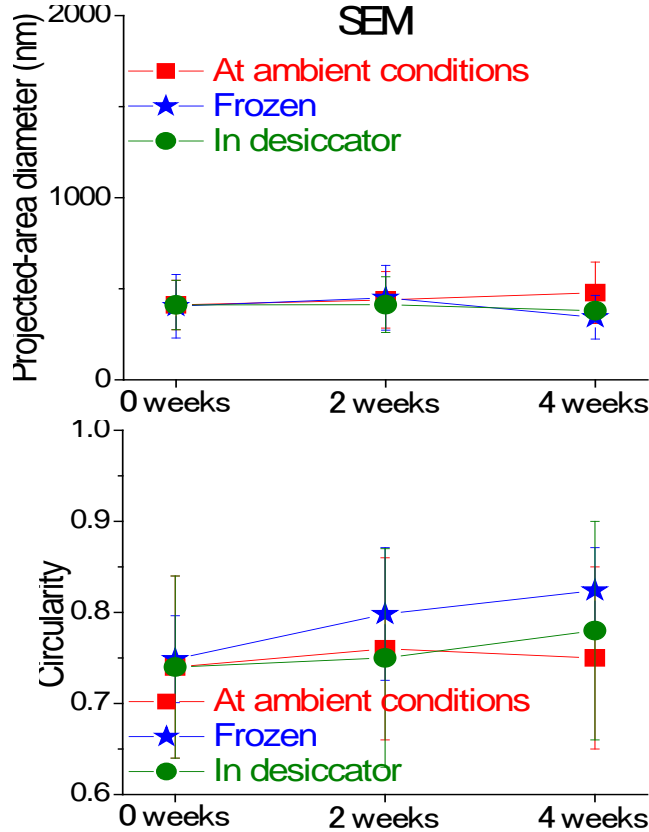
Figure 4.9 The projected-area diameter and circularity measured for all particles imaged using the SEM. As shown, there is little difference between the ambient, frozen, and desiccator conditions in terms of projected area diameter, but circularity increases in the frozen samples. (Figure adapted from Laskina et al., 2015).

Furthermore, the results from model system studies, i.e. the samples generated from a solution of 2:1 NaCl/malonic acid, are shown in Figures 4.8 and 4.9. The images shown in Figure 4.8 show fractionated and oddly shaped particles created from the desiccator and freezer. Most particles, from both the desiccator and freezer, were observed to contain some water when being viewed in the SEM, even though they were under vacuum. These observations were not seen in the imaging of the ambient samples. Figure 4.9 shows very little difference from the perspective of values determined for particle of desiccator and ambient samples in term of diameter and circularity. Additionally, the diameter of the measured particles were in line with those seen for the other samples, as discussed above. However, there is a slight, but significant, difference seen in the circularity of frozen samples for this model system. This may be due to moderately high

hygroscopic properties of malonic acid [Peng et al., 2001], causing the particles to retain more water than the other NaCl/malonic acid samples. Additionally, this shows that the SSA particles generated from the MART experiment have a less hygroscopic nature than those created from the NaCl/malonic acid model system, due to the differences seen in frozen samples when compared to the ambient condition samples of both the SSA and model system.

The results of the SEM analysis on these samples, by itself alone is insufficient to really prove anything in terms of storage conditions. However, when combined with analysis from Raman OM and AFM, it becomes apparent that storage of aerosol samples at ambient conditions (~20% RH, 22 °C) is best and does not show any aging effects in term of size or morphology. However, the common practice of storing samples in freezing condition, in most cases, show a small but significant change in both size and shape of particles, attributed to the water uptake of the particles during the freeze-thaw cycles. It appears that the more cycles, the further the particles deviate from the original dimensions. The differences in particles becomes clearer when comparing SEM images, as well. Therefore, it was concluded that the best method for aerosol sample storage is at ambient conditions.

4.3 WETSEM Capsules

As demonstrated in Section 4.2, SEM analysis of aerosol samples is limited due to the vacuum conditions of the sample chamber. The vacuum setting of SEMs can cause significant shrinkage of particles, up to 20-30% of the original size [Laskina et al., Unpublished work]. There are ways to combat this reduction, such as using cryo-capable electron microscopes or environmental electron microscopes. Furthermore, environmental electron microscopes often producing lower resolution images, due to the introduction of air in the sample chamber, which hinders the performance of the electron beam, frequently causing arcing within the instrument if

49
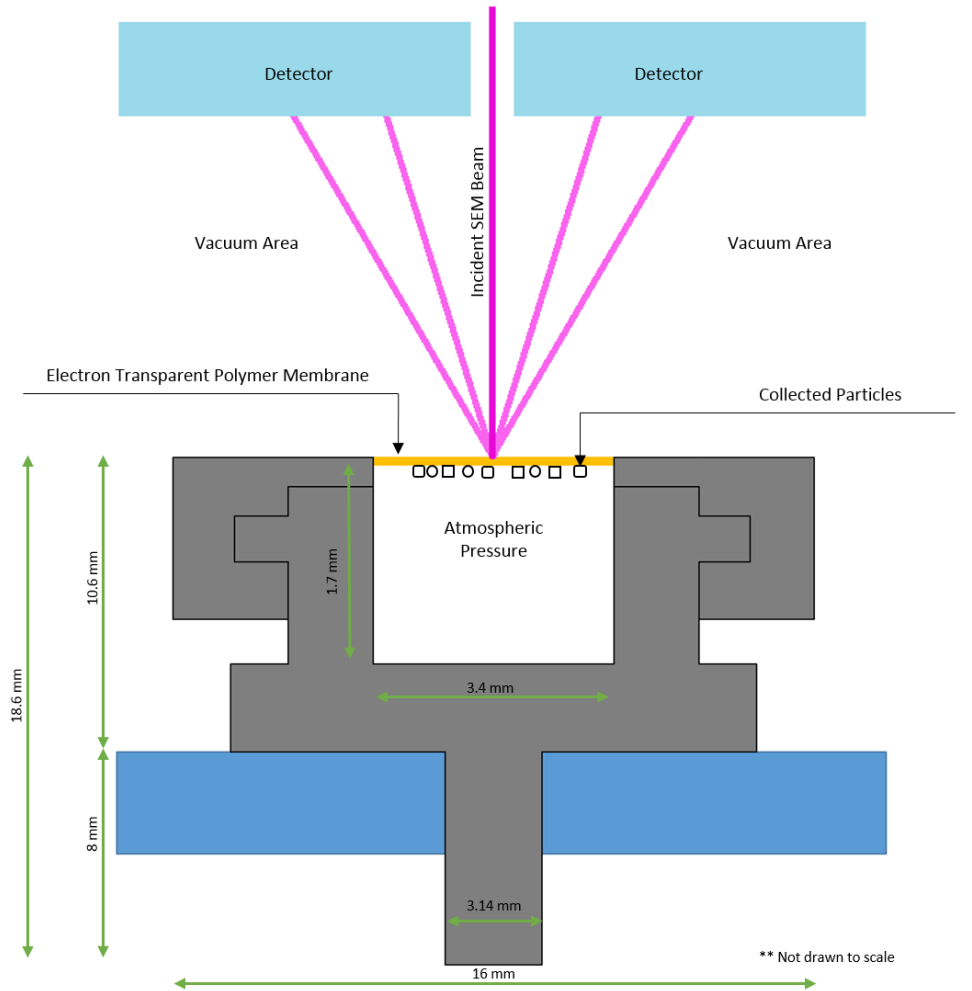
Figure 4.10 Schematic of the Quantomix QX-102 WETSEM capsules used for SEM analysis of particles trapped in ambient conditions.

not used properly. Here a technique to study encapsulated aerosol samples in an ambient environment while in a vacuum chamber of a scanning electron microscope, Quantomix QX-102 WETSEM capsules were tested and developed.

4.3.1 Experimental Setup

Aerosol particles are formed by atomizing (TSI Inc., Model 3076) solutions in Optima water (Fisher Scientific). Sodium chloride (NaCl) and potassium chloride (KCl) are purchased from Fisher Scientific (all ≥99.0%); magnesium chloride hexahydrate ($MgCl_2 \cdot 6H_2O$) and calcium chloride dihydrate ($CaCl_2 \cdot 2H_2O$) are purchased from Sigma-Aldrich (all ≥99.0%). All chemicals
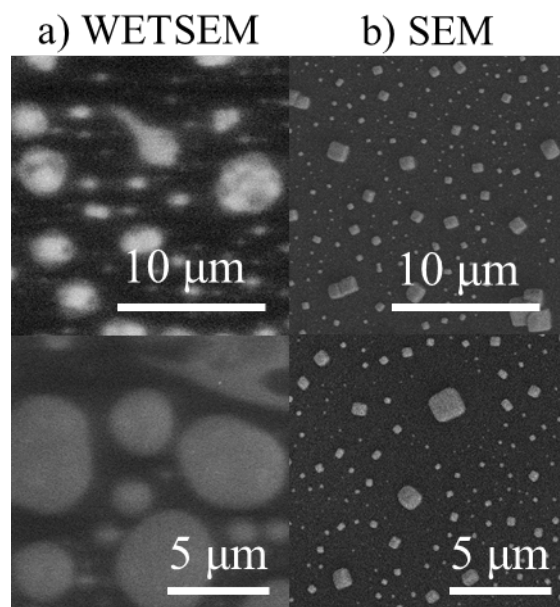
Figure 4.11 SEM Images on the left are NaCl/malonic acid aerosol samples deposited on the lid of a WETSEM capsule. On the right, SEM images of the same sample, only exposed to the vacuum environment of the SEM. (Figure taken from Laskina et al., 2015).

are used without further purification. Pure NaCl particles are prepared by atomizing solutions containing 0.5 wt. % of the salt. Mixture of chlorides are prepared from solution of NaCl, $MgCl_2 \cdot 6H_2O$, $CaCl_2 \cdot 2H_2O$ and KCl with a ratio of Na^+, Mg^{2+}, Ca^{2+}, K^+ = 1:0.11:0.02:0.02 wt. %, respectively. Upon exiting the atomizer, aerosols with a flow rate of 1.5 lpm are passed through diffusion dryer (TSI Inc., Model 3062) to reduce RH to <5% [Laskina et al., 2015]. Aerosol samples were collected directly into a Quantomix QX-102 WETSEM capsule, shown in Figure 4.10, for 3-5 minutes upon exiting the diffusion dryer. WETSEM capsules were originally created in order to conduct electron microscopy on liquid samples, however, this work will be the first to show that they can be used as a tool in aerosol studies to view particles in a more natural setting, as opposed to the vacuum chamber on an SEM.

SEM images were collected using a Hitachi S-4800 Scanning Electron Microscope, at a 20 kV accelerating voltage, a 10 μA beam current, and a 10 mm working distance in order to compensate for the extra height of the capsule.

51
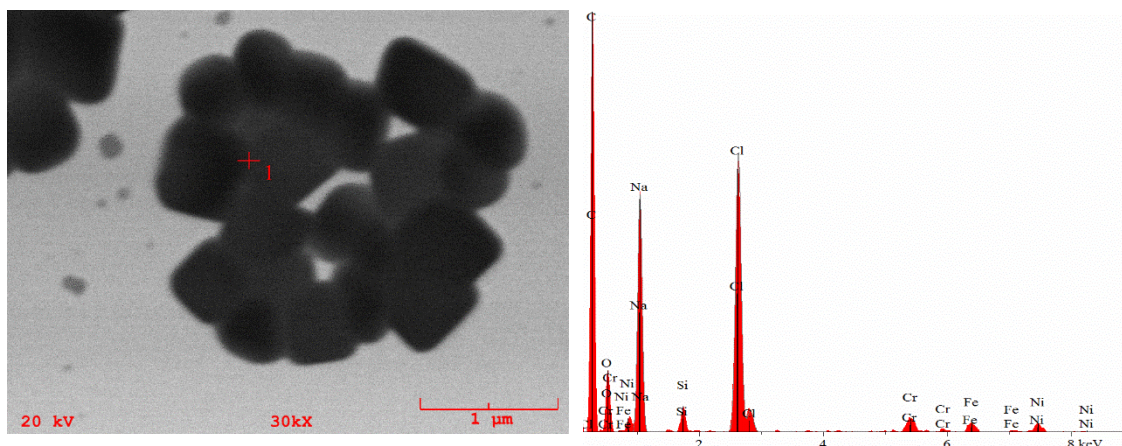
Figure 4.12 A sample spectra of a pure NaCl sample collected in a WETSEM capsule. The spectra shows no signal interference from the capsule, except for a few minor background peaks.

4.3.2 Results and Discussion

It is often most desirable to study samples in their natural environment. For atmospherically relevant aerosol particles, this means in equilibrium with the gas phase that surrounds it. On the left hand side of Figure 4.11 are images at two different magnifications of NaCl/malonic acid aerosol samples. These particles are contained within the WETSEM capsule. As can be seen, the particles are round droplet like particles. The image is somewhat distorted due to a combination of the charging of the electron beam on the liquid and the presence of organics, which are also poor conductors. To the best of our knowledge, these images are the first images taken of fully hydrated particles in a vacuumed SEM chamber. On the right hand side of Figure 4.11, images of the same sample, from the same WETSEM capsule, only now the lid has been taken off, therefore exposing the aerosols to the vacuum of the SEM sample chamber. The sample was exposed to the vacuum for less than 5 minutes, but in that short amount of time, the aerosols have effloresced, i.e. undergone crystallization and loss of water, in to the smaller, cubic structures that are normally associated with most salt like crystals.

In addition to imaging, another important complementary technique is EDX. Figure 4.12 shows an example spectra collected from pure NaCl aerosols collected and entrapped within a

52
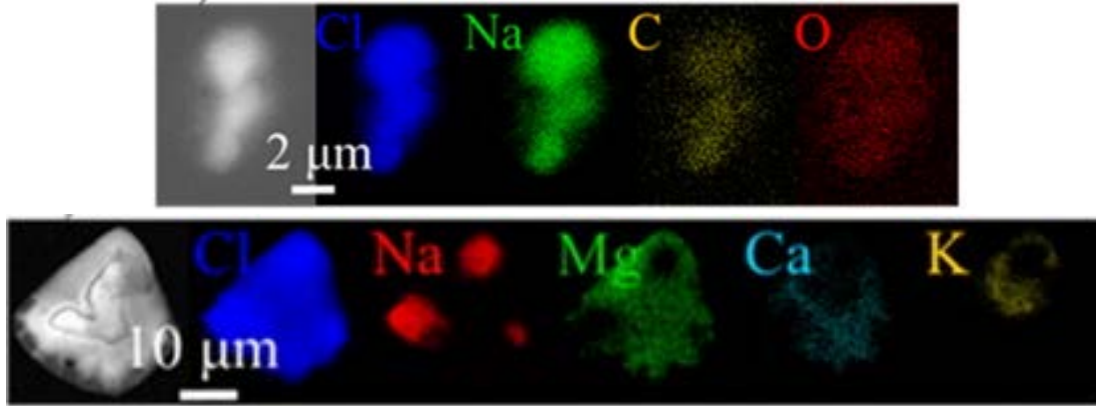
Figure 4.13 Two maps of two different particles showing the elemental mapping capabilities of particles in a WETSEM capsule. (Figure taken from Laskina et al., 2015).

WETSEM capsule. The spectrum shows some metal background peaks of the sample holder itself (Cr, Fe, Ni, and Si). The spectrum also shows carbon and oxygen signals from the polymer film that creates the transparent barrier between the inside of the capsule and vacuum environment. Although present in some cases, qualitative conclusions can be drawn from these signals based on ratios, because, by definition of a polymer, the ratio of carbon to oxygen signal should always be about the same, unless there is signal actually coming from the sample. While there should be caution used, it is possible to get qualitative measurements of organic components of a sample in a WETSEM capsule. Regardless, the peaks from the capsule itself do not interfere with the signal from other elements present in the particles of interest. The NaCl aggregate shown gives clear Na and Cl signals. Although the Cl:Na is higher than the expected 1:1 ratio, this has been observed for larger particles [Laskin et al., 2006]. A correction factor is not needed, because within experimental scatter, higher values like this have been measure, but the average measured values of Cl/Na over a population will closely match the unity value of 1:1 [Laskin et al., 2012].

Figure 4.13 shows two different maps of lab generated particles in a WETSEM capsule. The top is an organic mixture of NaCl and malonic acid, showing that Na and Cl show up very clearly, in addition to C and O, despite the polymer film of the capsule. The bottom map is an

53
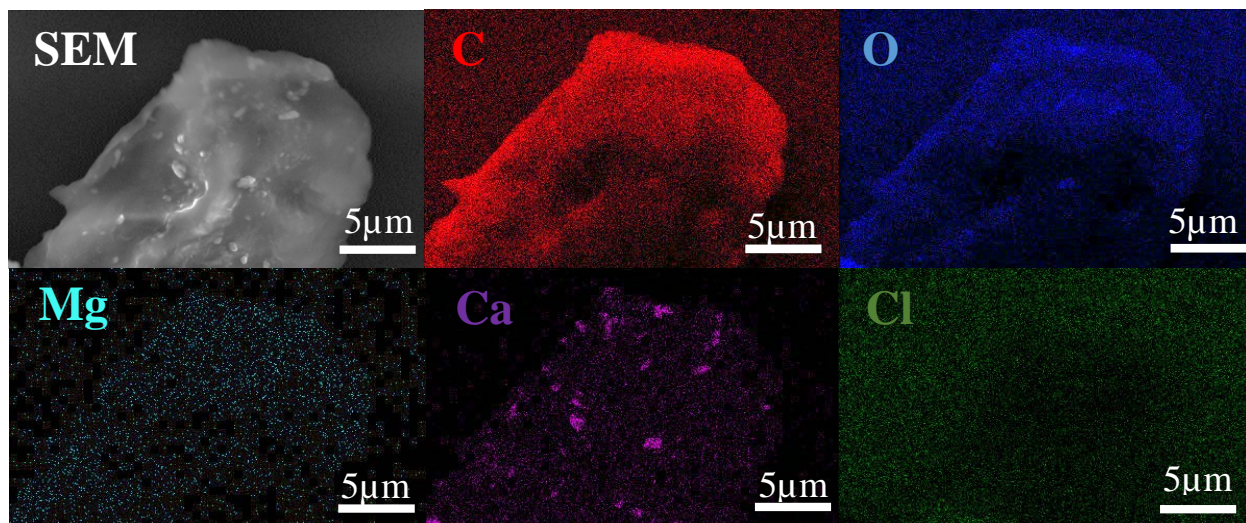
Figure 4.14 Elemental maps of a particle contained within a WETSEM capsule, filled with a sample of sea surface microlayer from the IMPACTS experiment.

aerosol generated from a mixture of four different chlorides. It is also important to note that the charging seen in the image of this large particle indicates that it was still wet upon mapping.

Lastly, Figure 4.14 is an elemental map of a particle in a liquid sample of the sea surface microlayer from the IMPACTS experiment, described in Chapter 3. The maps indicate the particle mostly consists of carbon, oxygen, and magnesium, while being devoid of any chlorine associated with the particle. It is possible that this particle is a polymer gel, as in previous work, it has been shown that the anionic nature of marine organic matter is bridged together by divalent cations to drive a polymer gel coalescence [Wells, 1998]. Interestingly, there also appears to be numerous calcium carbonate particles contained within the gel. This is an intriguing because there has been very little evidence of calcium carbonate particles reaching the aerosol phase from the wave flume. Regardless, the figure demonstrates another aspect of how WETSEM capsules can be used in sea spray aerosol research.

While the technique of using WETSEM capsules to study atmospheric aerosol particles in atmospherically relevant conditions, within a vacuum sample chamber, is not yet perfected, this is

a huge first step in bridging the gap between the laboratory settings of analysis techniques and real world conditions and is an exciting and promising innovation in aerosol research.

CHAPTER 5 – CONCLUSION

This work explored many different aspects of aerosol chemistry and analysis. In particular, sea spray aerosol particles were the main focal point of this research. Sea spray particles are one of the largest contributors to the atmospheric aerosol population, conservatively estimated at over 1300 Tg/year reaching the atmosphere [Hinds, 1999]. Despite oceans cover over 71% of the Earth's surface, sea spray aerosols are still considered to be a relative unknown in the extent of their impact on the Earth's atmosphere and radiative budget. This is, at least in part, due to the limited availability of pristine samples for analysis because even in the remote portions of the ocean, background pollutants are still present [Prather et al., 2013]. Recently, however, Prather, Bertram, Grassian, and colleagues were successful in breaking down this barrier by bringing the ocean into the laboratory setting, including the proper wave breaking, bubble bursting, sea spray aerosol generation mechanism [2013]. While it was an exciting new pathway that progressed the field drastically, it brought with it many questions to be answered. In this thesis, we attempted to answer some of those questions.

In order for support for hypothesis and conclusions to be made for interesting trends seen in field samples, first the ground work needed to be laid by using model systems. In Chapter 2, model systems consisting of simple carboxylic acids with varying degrees of chain lengths and reactive hydroxyl groups, which are common ocean surfactants, were studied in their interaction with common NaCl. Malic, hexanoic, nonanoic, and palmitic acids were all studied in three different molar concentrations with NaCl; 3:1, 1:1, and 1:3. It was found that the acid and NaCl will react and results in a chlorine depletion in the collected particles, evident by a less than expected 1:1 level of chlorine to sodium signal detected by energy dispersive x-ray spectroscopy. This result was expected, as it has been shown in recent literature that chlorine loss is possible

through a simple acid displacement mechanism that created HCl $_{(g)}$ and sodium salts [Laskin et al., 2012]. However, Laskin et al. attributed this displacement reaction as the result of sea spray aerosols reacting with secondary organic aerosol gasses. With this work, we hypothesized another reaction pathway for the chloride loss. We hypothesized that chlorine depletion in sea spray aerosols could also occur upon the formation of the aerosol, when carboxylic acids and NaCl are mixed together in small droplets. Additionally, it was shown that the level of chloride depletion has little correlation with the solubility of the modeled carboxylic acids, as even the least soluble acid (palmitic) showed similar Cl:Na levels as the more soluble, shorter chained mono-carboxylic acids. However, the levels of depletion were drastically different between the monocarboxylic acids and the dicarboxylic acids. All the molar concentrations of malic acid showed between a 75-100% decrease in chlorine levels when compared to sodium, whereas the monocarboxylic acids showed around a 20-25% reduction. Lastly, an interesting trend in morphology trends was seen in the collected particles. A common trend showed that the more chloride depleted a particle was, the more circular the particle became. This morphology change is an interesting finding that could have implications on the reactivity and transport of these particles in the atmosphere. In future works, in order to further clear up selectivity questions regarding chain length vs. the number of carboxylic acids/hydroxyl groups, other ocean surfactants should be studies, such as acetic acid (C-2, monocarboxylic), butyric acid (C-4, monocarboxylic), malic acid (C-3, dicarboxylic), and succinic acid (C-4, dicarboxylic). Additionally, experiments should be done on how the chloride depletion of particles affects their atmospherically relevant properties, such as water uptake abilities and optical properties.

As mentioned above, some of the findings in Chapter 2 helped lay the foundations for helping to explain the trends seen in the studies discussed in Chapter 3. This chapter delved into

actual field samples of sea spray aerosol particles, generated by an indoor waveflume in order to create background free samples [Prather et al., 2013]. Aerosols were generated and collected for over a month in a waveflume during the summer of 2014 at the Scripps Institute of Oceanography in La Jolla, CA. Upon offline analysis of these samples, it was shown that the aerosols generated during a specific day of the biological bloom were chloride depleted, similar to what was shown in the model system from Chapter 2. Interestingly, this drop in chlorine levels in particles corresponded to the peak of the biological activity in the waveflume. It is well known that biological species tend to produce organic compounds and excrete them into the ocean waters, including carboxylic acids [Adams et al., 2013]. With the absence of any secondary organic aerosols within the wave channel and little time to react even if there was, these results help to support our hypothesis that chlorine depletion in sea spray aerosols can, in fact, become chloride depleted upon the formation of the aerosol. While studies are still being conducted on the massive IMPACTS experiment and it is not yet known what compounds were on the surface water, this finding is critical in learning more about how the sea surface chemistry of the ocean helps dictate the chemical complexity of sea spray particles and therefore how it will interact within the atmosphere. Once the remaining few questions have been answered, this reaction mechanism should be taken into account in aerosol models and how they impact the atmosphere.

In the final research chapter, three different advances in the aerosol production, storage, and analysis were made. First in Chapter 4, we were able to use microscopy techniques to show that the current most popular generation method, via sintered glass filters, does a poor job of replicating actually real world sea spray aerosol samples. Instead, it was proven that a plunging waterfall method created particles that were more alike to the particles produced by the natural wave breaking method seen in ocean's [Collins et al., 2014]. Secondly, the common practice of

58

storing aerosol samples in freezing conditions in order to preserve the pristine conditions was challenged. In this study, samples stored in three different storage conditions (ambient, freezer, and desiccator) were analyzed using three different microscopy techniques (SEM, Raman, and AFM). Through combined results of all three techniques, it was proven that the popular freezing method is not the best way to keep collected field samples in storage. We showed that the best way to store samples is in controlled ambient laboratory conditions, around 22 °C and ~20% RH. Lastly, in order to overcome the obstacle of analyzing atmospheric particles in a vacuum setting, which causes drying out of the particles and evaporation of highly volatile species that may be present, we showed that we could collect, image, and obtain chemical data from atmospheric particles collected within a WETSEM capsule [Laskina et al., 2015]. This new method allows for researchers to be able to study atmospheric particles in atmospherically relevant conditions, something that has not been shown in literature before without the use of an expensive environmental electron microscope.

This work over the past couple years provided a few insights into the study of sea spray aerosols. In the beginning, the goal was to help bridge the gap in our lack of understanding of how sea spray aerosols play a role in our ever changing atmosphere. In order to fully understand the extent these particles play in atmospheric process', such as global warming and cloud formation, more studies must be conducted. However, this work was able to advance the work in the field by providing some fundamental answers and advancements in the area of sea spray aerosol chemistry.

REFERENCES

CHAPTER 1 – INTRODUCTION REFERENCES

1. Boucher, O.; Randall, D.; Artaxo, P.; Bretherton, C.; Feingold, G.; Forster, P.; Kerminen, V. M.; Kondo, Y.; Liao, H.; Lohmann, U.; Rasch, P.; Satheesh, S. K.; Sherwood, S.; Stevens, B.; Zhang, X. Y. Clouds and Aerosols. In *Climate Change 2013: The Physical Science Basis. Contribution of Working Group I to the Fifth Assessment Report of the Intergovernmental Panel on Climate Change*; Stocker, T.F., Qin, D., Plattner, G. K., Tignor, M., Allen, S. K., Boschung, J., Nauels, A., Xia, Y., Bex, V., Midgley, P. M., Eds.; Cambridge University Press: Cambridge, UK and New York, NY, 2013; pp. 571–658.

2. Pacyna, J. M. Sources, Particle Size Distribution and Transport of Aerosols. In *Airborne Particulate Matter*; Kouimtzis, T., Samara, C., Eds.; Springer-Verlag Berlin Heidelberg: New York, 1995.

3. Viana, M.; Pey, J.; Querol, X.; Alastuey, A.; De Leeuw, F.; Lükewille, A. Natural Sources of Atmospheric Aerosols Influencing Air Quality across Europe. *Sci. Total. Environ.* **2014,** 472; pp 825–833.

4. Albritton, D. L.; DeCola, P. L.; Anderson, D. E.; Fahey, D. W.; Gleason, J. F.; Keating, T. J.; Kruger, D. W.; Kurylo, M. J.; Levy,. J. M.; et al. Atmospheric Composition. In *Strategic Plan for the U.S. Climate Change Science Program*. U.S. Climate Change Science Program: Washington, D.C., 2003; pp. 30.

5. Hinds, W. C. *Aerosol Technology: Properties, Behavior, and Measurements of Airborne Particles*, 2nd ed.; John Wiley & Sons, Inc.: Hoboken, NJ, 1999.

6. Stocker, T. F.; Qin, D.; Plattner, G. K.; Alexander, L. V.; Allen, S. K.; Bindoff, N. L.; Bréon, F. M.; Church, J. A.; Cubasch, U.; Emori, S.; et al. Technical Summary. In *Climate Change 2013: The Physical Science Basis. Contribution of Working Group I to the Fifth Assessment Report of the Intergovernmental Panel on Climate Change*; Stocker, T.F., Qin, D., Plattner, G. K., Tignor, M., Allen, S. K., Boschung, J., Nauels, A., Xia, Y., Bex, V., Midgley, P. M., Eds.; Cambridge University Press: Cambridge, UK and New York, NY, 2013; pp. 33–115.

7. Forster, P.; Ramaswamy, V.; Artaxo, P.; Berntsen, T.; Betts, R.; Fahey, D. W.; Haywood, J.; Lean, J.; Lowe, D. C.; Myhre, G.; et al. Changes in Atmospheric Constituents and in Radiative Forcing. In *Climate Change 2007: The Physical Science Basis. Contribution of Working Group I to the Fourth Assessment Report of the Intergovernmental Panel on Climate Change*; Solomon, S., Qin, D., Manning, M., Chen, Z., Marquis, M., Averyt, K. B., Tignor, M., Miller, H. L., Eds. Cambridge University Press: Cambridge, UK and New York, NY, 2007.

8. Penner, J. E.; Andreae, M.; Annegarn, H.; Barrie, l.; Feichter, J.; Hegg, D.; Jayaraman, A.; Leaitch, R.; Murphy, D.; Nganga, J.; Pitari, G.; et al. Aerosols, their Direct and Indirect Effects. In *Climate Change 2001: The Physical Science Basis. Contribution of Working Group I to the Third Assessment Report of the Intergovernmental Panel on Climate Change*; Houghton, J. T., Ding, Y., Griggs, D. J., Nouger, M., van der Linden, P. J., Dai, X., Maskell, K., Johnson, C. A., Eds. Cambridge University Press: Cambridge, UK and New York, NY, 2013; pp 291-336.

9. Seinfeld, J. H.; Pandis, S. N. *Atmospheric Chemistry and Physics: From Air Pollution to Climate Change*, 2nd ed.; John Wiley & Sons, Inc.: Hoboken, NJ, 2006.

10. Rosenfeld, D.; Woodley, W. L. Pollution and Clouds. *Physics* World; Institute of Physics Publishing LTD: Bristol, UK, 2001; pp 33–37.

11. Denman, K. L.; Brasseur, G.; Chidthaisong, A.; Ciais, P.; Cox, P. M.; Dickinson, R. E.; Hauglustaine, D.; Heinze, C.; Holland, E.; et al. Couplings between Changes in the Climate System and Biogeochemistry. In *Climate Change 2007: The Physical Science Basis. Contribution of Working Group I to the Fourth Assessment Report of the Intergovernmental Panel on Climate Change*; Solomon, S., Qin, D., Manning, M., Chen, Z., Marquis, M., Averyt, K. B., Tignor, M., Miller, H. L., Eds. Cambridge University Press: Cambridge, UK and New York, NY, 2007.

12. Goosse H.; Barriat, P. Y.; Lefebvre, W.; Loutre, M. F.; Zunz, V. The Response of the Climate System to a Perturbation. In *Introduction to Climate Dynamics and Climate Modeling* [Online]; Cambridge University Press: Cambridge, UK, 2008. http://www.climate.be/textbook/index.html (accessed May 22, 2015).

13. IPCC. Summary for Policymakers. In *Climate Change 2013: The Physical Science Basis. Contribution of Working Group I to the Fifth Assessment Report of the Intergovernmental Panel on Climate Change*; Stocker, T.F., Qin, D., Plattner, G. K., Tignor, M., Allen, S. K., Boschung, J., Nauels, A., Xia, Y., Bex, V., Midgley, P. M., Eds.; Cambridge University Press: Cambridge, UK and New York, NY, 2013.

14. Laskin, A.; Moffet, R. C.; Gilles, M. K.; Fast, J. D.; Zaveri, R. A.; Wang, B.; Nigge, P.; Shutthanandan, J. Tropospheric Chemistry of Internally Mixed Sea Salt and Organic Particles: Surprising Reactivity of NaCl with Weak Organic Acids. *J. Geophys. Res.* **2012,** 117, D15302.

15. Wex, H.; Fuentes, E.; Tsagkogeorgas, G.; Voigtländer, J.; Clauss, T.; Kiselev, A.; Green, D. H.; Coe, H.; McFiggans, G.; Stratmann, F. The Influence of Algal Exudate on the Hygroscopicity of Sea Spray Particles. *Adv. Meteor.* **2010,** *2010,* 365131.

16. Prather, K. A.; Bertram, T. H.; Grassian, V. H.; Deane, G. B.; Stokes, M. D.; DeMott, P. J.; Aluwihare, L. I.; Palenik, B. P.; Azam, F.; Seinfeld, J. H.; et al. Bringing the Ocean into the Laboratory to Probe the Chemical Complexity of Sea Spray Aerosol. *Proc. Natl. Acad. Sci. U.S.A.* **2013,** 110, 7550−7555.

17. Ault, A. P.; Zhao, D.; Ebben, C. J.; Tauber, M. J.; Geiger, F. M.; Prather, K. A.; Grassian, V. H. Raman Microspectroscopy and Vibrational Sum Frequency Generation Spectroscopy as Probes of the Bulk and Surface Compositions of Size-Resolved Sea Spray Aerosol Particles. *Phys. Chem. Chem. Phys.* **2013,** 15, 6206– 6214.

18. Stokes, M. D.; Deane, G. B.; Prather, K. A.; Bertram, T. H.; Ruppel, M. J.; Ryder, O. S.; Brady, J. M.; Zhao, D. A Marine Aerosol Reference Tank System as a Breaking Wave Analogue for the Production of Foam and Sea-Spray Aerosols. *Atmos. Meas. Tech.* **2013,** *6,* 1085.

19. Ault, A. P.; Moffet, R. C.; Baltrusaitis, J.; Collins, D. B.; Ruppel, M. J.; Cuadra-Rodriguez, L. A.; Zhao, D.; Guasco, T. L.; Ebben, C. J.; Geiger, F. M.; et al. Size-Dependent Changes in Sea Spray Aerosol Composition and Properties with Different Seawater Conditions. *Environ. Sci. Technol.* **2013,** 47, 5603−5612.

20. Collins, D. B.; Ault, A. P.; Moffet, R. C.; Ruppel, M. J.; Cuadra-Rodriguez, L. A.; Guasco, T. L.; Corrigan, C. E.; Pedler, B. E.; Azam, F.; Aluwihare, L. I.; Bertram, T. H.; Roberts, G. C.; Grassian, V. H.; Prather, K. A. Impact of Marine Biogeochemistry on the Chemical Mixing State and Cloud Forming Ability of Nascent Sea Spray Aerosol. *J. Geophys. Res.-Atmos.* **2013,** 118, 8553−8565.

21. Ebben, C. J.; Ault, A. P.; Ruppel, M. J.; Ryder, O. S.; Bertram, T. H.; Grassian, V. H.; Prather, K. A.; Geiger, F. M. Size-Resolved Sea Spray Aerosol Particles Studied by Vibrational Sum Frequency Generation. *J. Phys. Chem. A* **2013,** 117, 6589−6601.

22. Guasco, T. L.; Cuadra-Rodriguez, L. A.; Pedler, B. E.; Ault, A. P.; Collins, D. B.; Zhao, D.; Kim, M. J.; Ruppel, M. J.; Wilson, S. C.; Pomeroy, R. S.; Grassian, V. H.; Azam, F.; Bertram, T. H.; Prather, K. A. Transition metal associations with primary biological particles in sea spray aerosol generated in a wave channel. *Environ. Sci. Technol.* **2014,** 48, 1324−1333.

23. Collins, D. B.; Zhao, D. F.; Ruppel, M. J.; Laskina, O.; Grandquist, J. R.; Modini, R. L.; Stokes, M. D.; Russell, L. M.; Bertram, T. H.; Grassian, V. H.; et al. Direct Aerosol Chemical Composition Measurements to Evaluate the Physicochemical Differences between Controlled Sea Spray Aerosol Generation Schemes. *Atmos. Meas. Technol. Discuss.* **2014,** *7,* 6457−6499.

24. Laskina, O.; Morris, H.; Grandquist, J. R.; Qin, Z.; Stone, E. A.; Tivanski, A. V.; Grassian, V. H. Size Matters in the Water Uptake and Hygroscopic Growth of Atmospherically Relevant Multicomponent Aerosol Particles. *J. Phys. Chem. A*, **2015,** 119 (19), 4489–4497.

25. Wang, X.; Sultana, C. M.; Trueblood, J.; Hill, T. C. J.; Malfatti, F.; Lee, C.; Laskina, O.; Moore, K. A.; Beall, C. M.; McCluskey, C. S.; Cornwell, G. C.; Zhou, Y.; Cox, J. L.; Pendergraft, M. V.; Bertram, T. H.; Cappa, C. D.; DeMott, P. J.; Grassian, V. H.; Prather, K. A. Microbial Control of Sea Spray Aerosol Composition: A Tale of Two Blooms. *ACS Cent. Sci.*, **2015**.

CHAPTER 2 – MODEL SYSTEMS REFERENCES

1. Finlayson-Pitts, B. J. The Tropospheric Chemistry of Sea Salt: A Molecular-Level View of the Chemistry of NaCl and NaBr. *Chem. Rev.* **2003,** 103, 4801−4822.

2. Laskin, A.; Moffet, R. C.; Gilles, M. K.; Fast, J. D.; Zaveri, R. A.; Wang, B.; Nigge, P.; Shutthanandan, J. Tropospheric Chemistry of Internally Mixed Sea Salt and Organic Particles: Surprising Reactivity of NaCl with Weak Organic Acids. *J. Geophys. Res.* **2012,** 117, D15302.

3. Laskin, A.; Iedema, M. J.; Cowin, J. P. Quantitative Time-Resolved Monitoring of Nitrate Formation in Sea Salt Particles Using a CC-SEM/EDX Single Particle Analysis. *Environ. Sci. Technol.* **2002,** 36 (23), 4948−4955.

4. Laskin, A.; Iedema, M. J.; Ichkovich, A.; Graber, E. R.; Taraniuk, I.; Rudich, Y. Direct Observation of Completely Processed Calcium Carbonate Dust Particles. *Faraday Discuss.* **2005,** 130, 453−468.

5. Newberg, J. T.; Matthew, B. M.; Anastasio, C. Chloride and Bromide Depletions in Sea Salt Particles over the Northeastern Pacific Ocean. *J. Geophys. Res.* **2005,** 110, D06209.

6. Keene, W. C.; Pszenny, A. A. P.; Jacob, D. J.; Duce, R. A.; Galloway, J. N.; Schultz-Tokos, J. J.; Sievering, H.; Boatman, J. F. The Geochemical Cycling of Reactive Chlorine through the Marine Troposphere. *Global Biogeochem. Cycles* **1990,** 4, 407−430.

7. Kerminen, V.-M.; Teinila, K.; Hillamo, R.; Pakkanen, T. Substitution of Chloride in Sea-Salt Particles by Inorganic and Organic Anions. *J. Aerosol Sci.* **1998,** 29, 929−942.

8. Meeuse, B. J. D. Free Sulfuric Acid in the Brown Alga, Desmarestia. *Biochem. Biophys. Acta.* **1956,** 19, 372.

9. Meeuse, B. J. D. Storage Products. In *Physiology and Biochemistry of Algae;* Lewin, R. A., Ed.; Academic Press: New York, 1962.

10. van Pinxteren, M.; Muller, C.; Iinuma, Y.; Stolle, C.; Herrmann, H. Chemical Characterization of Dissolved Organic Compounds from Coastal Sea Surface Microlayers (Baltic Sea, Germany). *Environ. Sci. Technol.* **2012,** 46, 10455−10462.

11. Kawamura, K.; Semere, R.; Imai, Y.; Fujii, Y.; Hayashi, M. Water Soluble Dicarboxylic Acids and Related Compounds in Antarctic Aerosols. *J. Geophys. Res. Atmos.* **1996,** 101, 18721−18728.

12. Kawamura, K.; Sakaguchi, F. Molecular Distributions of Water Soluble Dicarboxylic Acids in Marine Aerosols over the Pacific Ocean Including Tropics. *J. Geophys. Res. Atmos.* **1999,** 104, 3501−3509.

13. Kawamura, K.; Usukura, K. Distributions of Low Molecular Weight Dicarboxylic Acids in the North Pacific Aerosol Samples. *J. Oceanogr.* **1993,** 49, 271−283.

14. de Leeuw, G.; Andreas, E. L.; Anguelova, M. D.; Fairall, C. W.; Lewis, E. R.; O'Dowd, C.; Schulz, M.; Schwartz, S. E. Production Flux of Sea Spray Aerosol. *Rev. Geophys.* **2011,** 49.

15. Miñambres, L.; Mendez, E.; Sanchez, M. N.; Castano, F.; Basterretxea, F. J. The Effect of Low Solubility Organic Acids on the Hygroscopicity of Sodium Halide Aerosols. *Atmos. Chem. Phys.* **2014,** 14, 11409.

16. Lawler, M. J.; Whitehead, J.; O'Dowd, C.; Monahan, C.; McFiggans, G.; Smith, J. N. Composition of 15–85 nm Particles in Marine Air. *Atmos. Chem. Phys.* **2014,** 14, 11557-11569.

17. Zhang, Z.; Liu, L.; Liu, C.; Cai, W. Studies on the Sea Surface Microlayer II. The Layer of Sudden Change of Physical and Chemical Properties. *J. Colloids Interface Sci.* **2003**, *264*, 148–159.

18. Kegley, S.; Conlisk, E.; Moses, M. *Marin Municipal Water District Herbicide Risk Assessment;* Technical Report for the Marin Municipal Water District Vegetation Management Plan; Pesticide Research Institute: Berkley, CA, January 2010; 7-3.

19. Goecke, F.; Hernandez, V.; Bittner, M.; Gonzalez, M.; Becerra, J.; Silva, M. Fatty Acid Composition of Three Species of Codium (Bryopsidales, Chlorophyta) in Chile. *Rev. Biol. Mar. Oceanogr.* **2010,** 45, 325-330.

20. Adams, E. M.; Allen, H. C. Palmitic Acid on Salt Subphases and in Mixed Monolayers of Cerebrosides: Application to Atmospheric Aerosol Chemistry. *Atmosphere (Basel)* **2013,** 4, 315−336.

CHAPTER 3 – IMPACTS BIOLOGICAL BLOOM EXPERIMENT

1. Prather, K. A.; Bertram, T. H.; Grassian, V. H.; Deane, G. B.; Stokes, M. D.; DeMott, P. J.; Aluwihare, L. I.; Palenik, B. P.; Azam, F.; Seinfeld, J. H.; et al. Bringing the Ocean into the Laboratory to Probe the Chemical Complexity of Sea Spray Aerosol. *Proc. Natl. Acad. Sci. U.S.A.* **2013,** 110, 7550−7555.

2. *Impacts of Climate Change on the Occurrence of Harmful Algal Blooms;* EPA 820-S-13-001; U.S. Environmental Protection Agency: U.S. Government Printing Office: Washington, DC, 2013.

3. Diersing, N. *Phytoplankton Blooms: The Basics;* Florida Keys National Marine Sanctuary, National Oceanic and Atmospheric Administration: Washington, DC, May 2009. http://floridakeys.noaa.gov/scisummaries/wqpb.pdf (accessed April 9, 2015).

4. Putnam, W. *Portrait of Global Aerosols;* NASA/Goddard, 2013. https://www.nasa.gov/multimedia/imagegallery/image_feature_2393.html#.VS_aIqO5LAc (accessed April 9, 2015).

5. Creamean, J. M.; Suski, K. J.; Rosenfeld, D.; Cazorla, A.; DeMott, P. J.; Sullivan, R. C.; White, A. B.; Ralph, F. M.; Minnis, P.; Comstock, J. M.; et al. Dust and Biological Aerosols from the Sahara and Asia Influence Precipitation in the Western U.S. *Science* **2013,** 339, 1572−1578.

6. Becker, J. W.; Berube, P. M.; Follett, C. L.; Waterbury, J. B.; Chisholm, S. W.; DeLong, E. F.; et al. Closely Related Phytoplankton Species Produce Similar Suites of Dissolved Organic Matter. *Front. Microbiol.* **2014,** 111, 5.

7. Wang, X.; Sultana, C. M.; Trueblood, J.; Hill, T. C. J.; Malfatti, F.; Lee, C.; Laskina, O.; Moore, K. A.; Beall, C. M.; McCluskey, C. S.; Cornwell, G. C.; Zhou, Y.; Cox, J. L.; Pendergraft, M. V.; Bertram, T. H.; Cappa, C. D.; DeMott, P. J.; Grassian, V. H.; Prather, K. A. Microbial Control of Sea Spray Aerosol Composition: A Tale of Two Blooms. *ACS Cent. Sci.*, **2015**.

8. Adams, E. M.; Allen, H. C. Palmitic Acid on Salt Subphases and in Mixed Monolayers of Cerebrosides: Application to Atmospheric Aerosol Chemistry. *Atmosphere (Basel)* **2013,** 4, 315−336.

9. Aller, J. Y.; Kuznetsova, M. R.; Jahns, C. J.; Kemp, P. F. The Sea Surface Microlayer as a Source of Viral and Bacterial Enrichment in Marine Aerosols. *Aerosol Sci.* **2005,** 36, 801–812.

10. Laskina, O.; Morris, H.; Grandquist, J. R.; Stone, E. A.; Tivanski, A. V.; Grassian, V. H. Substrate-deposited sea spray aerosol particles: Inter-comparison study of analytical method, substrate and storage conditions on particle size, phase and morphology. Unpublished work, 2015.

11. Boyer, J. N.; Kelble, C. R.; Ortner, P. B.; Rudnick, D. T. Phytoplankton Bloom Status: Chlorophyll a Biomass as an Indicator of Water Quality Condition in the Southern Estuaries of Florida, USA. *Ecol. Indic.* **2009,** 9S, S56–S67.

12. Czuba, J. A.; Magirl, C. S.; Czuba, C. R.; Grossman, E. E.; Curran, C. A.; Gendaszek, A. S.; Dinicola, R. S. Comparability of Suspended-Sediment Concentration and Total Suspended Solids Data Sediment Load from Major Rivers into Puget Sound and its Adjacent Waters. *USGS Fact Sheet* **2011,** 2011–3083.

13. Gagosian, R. B.; Lee, C. Processes Controlling the Distribution of Biogenic Organic Compounds in Seawater. In *Marine Organic Chemistry*; Duursma, E. K., Dawson, R., Eds.; Elsevier: New York, 1981; pp 91-124.

14. Becker, W. Microalgae in Human and Animal Nutrition. In *Handbook of Microalgal Culture: Biotechnology and Applied Phycology;* Richmond, A., Ed.; Blackwell Publishing Ltd: Oxford, UK, 2003.

15. Laskin, A.; Moffet, R. C.; Gilles, M. K.; Fast, J. D.; Zaveri, R. A.; Wang, B.; Nigge, P.; Shutthanandan, J. Tropospheric Chemistry of Internally Mixed Sea Salt and Organic Particles: Surprising Reactivity of NaCl with Weak Organic Acids. *J. Geophys. Res.* **2012,** 117, D15302.

16. Schenkel, L. C.; Bakovic, M. Formation and Regulation of Mitochondrial Membranes. *Int. J. Cell Biol.* **2014,** Article ID 709828.

17. Ault, A. P.; Moffet, R. C.; Baltrusaitis, J.; Collins, D. B.; Ruppel, M. J.; Cuadra-Rodriguez, L. A.; Zhao, D.; Guasco, T. L.; Ebben, C. J.; Geiger, F. M.; et al. Size-Dependent Changes in Sea Spray Aerosol Composition and Properties with Different Seawater Conditions. *Environ. Sci. Technol.* **2013,** 47, 5603−5612.

18. Wells, M. L. Marine Colloids: A Neglected Dimension. *Nature* **1998,** 391, 530–53.

CHAPTER 4 – METHOD DEVELOPMENT REFERENCES

1. Grythe, H.; Ström, J.; Krejci, R.; Quinn, P.; Stohl, A. A Review of Sea-Spray Aerosol Source Functions Using a Large Global Set of Sea Salt Aerosol Concentration Measurements. *Atmos. Chem. Phys.* **2014,** 14, 1277–1297.

2. Prather, K. A.; Bertram, T. H.; Grassian, V. H.; Deane, G. B.; Stokes, M. D.; DeMott, P. J.; Aluwihare, L. I.; Palenik, B. P.; Azam, F.; Seinfeld, J. H.; et al. Bringing the Ocean into the Laboratory to Probe the Chemical Complexity of Sea Spray Aerosol. *Proc. Natl. Acad. Sci. U.S.A.* **2013,** *110,* 7550−7555.

3. Collins, D. B.; Zhao, D. F.; Ruppel, M. J.; Laskina, O.; Grandquist, J. R.; Modini, R. L.; Stokes, M. D.; Russell, L. M.; Bertram, T. H.; Grassian, V. H.; et al. Direct Aerosol Chemical Composition Measurements to Evaluate the Physicochemical Differences between Controlled Sea Spray Aerosol Generation Schemes. *Atmos. Meas. Technol. Discuss.* **2014,** *7,* 6457−6499.

4. Keene, W. C.; Maring, H.; Maben, J. R.; Kieber, D. J.; Pszenny, A. A. P.; Dahl, E. E.; Izaguirre, M. A.; Davis, A. J.; Long, M. S.; Zhou, X. L.; Smoydzin, L.; Sander, R. Chemical and Physical Characteristics of Nascent Aerosols Produced by Bursting Bubbles at a Model Air-Sea Interface. *J. Geophys. Res., [Atmos.]* **2007,** *112* (D21).

5. Gaston, C. J.; Furutani, H.; Guazzotti, S. A.; Coffee, K. R.; Bates, T. S.; Quinn, P. K.; Aluwihare, L. I.; Mitchell, B. G.; Prather, K. A. Unique Ocean-Derived Particles Serve as a Proxy for Changes in Ocean Chemistry. *J. Geophys. Res. – Atmos.* **2011**, *116*, D18310.

6. Deane, G. B.; Stokes, M. D. Scale Dependence of Bubble Creation Mechanisms in Breaking Waves. *Nature* **2002**, *418* (6900), 839−844.

7. Stokes, M. D.; Deane, G. B.; Prather, K. A.; Bertram, T. H.; Ruppel, M. J.; Ryder, O. S.; Brady, J. M.; Zhao, D. A Marine Aerosol Reference Tank System as a Breaking Wave Analogue for the Production of Foam and Sea-Spray Aerosols. *Atmos. Meas. Tech.* **2013,** *6,* 1085.

8. Ault, A. P.; Moffet, R. C.; Baltrusaitis, J.; Collins, D. B.; Ruppel, M. J.; Cuadra-Rodriguez, L. A.; Zhao, D.; Guasco, T. L.; Ebben, C. J.; Geiger, F. M.; et al. Size-Dependent Changes in Sea Spray Aerosol Composition and Properties with Different Seawater Conditions. *Environ. Sci. Technol.* **2013,** 47, 5603−5612.

9. Laskin, A.; Cowin, J. P.; Iedema, M. J. Analysis of Individual Environmental Particles Using Modern Methods of Electron Microscopy and X-ray Microanalysis. *J. Electron Spectrosc. Relat. Phenom.* **2006,** 150, 260−274.

10. Willis, R. D.; Blanchard, F. T.; Conner, T. L. Guidelines for the Application of SEM/EDX Analytical Techniques to Particulate Matter Samples; EPA # 600/R-02/070; U.S. Environmental Protection Agency: Research Triangle, Park, NC, 2002.

11. Laskina, O.; Morris, H.; Grandquist, J. R.; Stone, E. A.; Tivanski, A. V.; Grassian, V. H. Substrate-Deposited Sea Spray Aerosol Particles: Inter-Comparison Study of Analytical Method, Substrate and Storage Conditions on Particle Size, Phase and Morphology. Unpublished work, 2015.

12. Peng, C.; Chan, M. N.; Chan, C. K. The Hygroscopic Properties of Dicarboxylic and Multifunctional Acids: Measurements and UNIFAC Predictions. *Environ. Sci. Technol.* **2001,** 35, 4495−4501.

13. Zardini, A. A.; Sjogren, S.; Marcolli, C.; Krieger, U. K.; Gysel, M.; Weingartner, E.; Baltensperger, U.; Peter, T. A Combined Particle Trap/HTDMA Hygroscopicity Study of Mixed Inorganic/Organic Aerosol Particles. *Atmos. Chem. Phys.* **2008,** 8, 5589−5601.

14. Laskina, O.; Morris, H.; Grandquist, J. R.; Qin, Z.; Stone, E. A.; Tivanski, A. V.; Grassian, V. H. Size Matters in the Water Uptake and Hygroscopic Growth of Atmospherically Relevant Multicomponent Aerosol Particles. *J. Phys. Chem. A*, **2015,** 119 (19), 4489–4497.

15. Laskin, A.; Moffet, R. C.; Gilles, M. K.; Fast, J. D.; Zaveri, R. A.; Wang, B.; Nigge, P.; Shutthanandan, J. Tropospheric Chemistry of Internally Mixed Sea Salt and Organic Particles: Surprising Reactivity of NaCl with Weak Organic Acids. *J. Geophys. Res.* **2012,** 117, D15302.

16. Wells, M. L. Marine Colloids: A Neglected Dimension. *Nature* **1998,** 391, 530–531.

CHAPTER 5 – CONCLUSION REFERENCES

1. Hinds, W. C. *Aerosol Technology: Properties, Behavior, and Measurements of Airborne Particles*, 2nd ed.; John Wiley & Sons, Inc.: Hoboken, NJ, 1999.

2. Prather, K. A.; Bertram, T. H.; Grassian, V. H.; Deane, G. B.; Stokes, M. D.; DeMott, P. J.; Aluwihare, L. I.; Palenik, B. P.; Azam, F.; Seinfeld, J. H.; et al. Bringing the Ocean into the Laboratory to Probe the Chemical Complexity of Sea Spray Aerosol. *Proc. Natl. Acad. Sci. U.S.A.* **2013,** 110, 7550−7555.

3. Laskin, A.; Moffet, R. C.; Gilles, M. K.; Fast, J. D.; Zaveri, R. A.; Wang, B.; Nigge, P.; Shutthanandan, J. Tropospheric Chemistry of Internally Mixed Sea Salt and Organic Particles: Surprising Reactivity of NaCl with Weak Organic Acids. *J. Geophys. Res.* **2012,** 117, D15302.

4. Adams, E. M.; Allen, H. C. Palmitic Acid on Salt Subphases and in Mixed Monolayers of Cerebrosides: Application to Atmospheric Aerosol Chemistry. *Atmosphere (Basel)* **2013,** 4, 315−336.

5. Collins, D. B.; Zhao, D. F.; Ruppel, M. J.; Laskina, O.; Grandquist, J. R.; Modini, R. L.; Stokes, M. D.; Russell, L. M.; Bertram, T. H.; Grassian, V. H.; et al. Direct Aerosol Chemical Composition Measurements to Evaluate the Physicochemical Differences between Controlled Sea Spray Aerosol Generation Schemes. *Atmos. Meas. Technol. Discuss.* **2014,** 7, 6457−6499.

6. Laskina, O.; Morris, H.; Grandquist, J. R.; Qin, Z.; Stone, E. A.; Tivanski, A. V.; Grassian, V. H. Size Matters in the Water Uptake and Hygroscopic Growth of Atmospherically Relevant Multicomponent Aerosol Particles. *J. Phys. Chem. A*, **2015,** 119 (19), 4489–4497.